Monitoring the extreme flood events in the Yangtze River Basin based on GRACE/GRACE-FO satellite data

Jingkai Xie[1], Yue-Ping Xu[1], Hongjie Yu[1], Yan Huang[2], Yuxue Guo[1]

[1]Institute of Hydrology and Water Resources, Zhejiang University, Hangzhou, 310058, China
[2]Changjiang Water Resources Commission of the Ministry of Water Resources, Wuhan, 43000, China

Correspondence to: Yue-Ping Xu (yuepingxu@zju.edu.cn)

Abstract. Gravity Recovery and Climate Experiment (GRACE) and its successor GRACE Follow-on (GRACE-FO) satellite provide terrestrial water storage anomaly (TWSA) estimates globally that can be used to monitor flood in various regions at monthly intervals. However, the coarse temporal resolution of GRACE/GRACE-FO satellite data has been limiting its applications at finer temporal scales. In this study, TWSA estimates have been reconstructed and then temporally downscaled into daily values based on three different learning-based models, namely multi-layer perceptron (MLP) model, long-short term memory (LSTM) model and multiple linear regression (MLR) model. Furthermore, a new index incorporating temporally downscaled TWSA estimates combined with daily average precipitation anomalies is proposed to monitor the severe flood events at sub-monthly time scales for the Yangtze River Basin (YRB), China. The results indicated that (1) the MLP model shows the best performance in reconstructing monthly TWSA with RMSE = 10.9 mm/month and NSE = 0.89 during the validation period; (2) the MLP model can be useful in temporally downscaling monthly TWSA estimates into daily values; (3) the proposed normalized daily flood potential index (NDFPI) facilitates robust and reliable characterization of severe flood events at sub-monthly time scales; (4) the flood events can be monitored by the proposed NDFPI earlier than traditional streamflow observations with respect to the YRB and its individual subbasins. All these findings can provide new opportunities for applying GRACE/GRACE-FO satellite data to investigations of sub-monthly signals and have important implications for flood hazard prevention and mitigation in the study region.

1 Introduction

Extreme floods, as one of the most destructive natural hazards, not only cause lots of casualties in China and around the world, but also have considerably wider and adverse economic consequences (Dottori et al., 2018). According to the report published by the United Nations Office for Disaster Risk Reduction (UNDRR), the total economic loss induced by floods is up to $651 billion (USD) worldwide from 2000 to 2019 (https://www.undrr.org/publication/human-cost-disasters-overview-last-20-years-2000-2019). Meanwhile, floods are projected to become more frequent and extreme under global warming as it can substantially amplify the water holding capacity of the air and increase the occurrence of extreme precipitation events

(Slater et al., 2016). Therefore, monitoring extreme flood events has long been a hot topic for hydrologists and decision
30 makers around the world (Tanoue et al., 2020; Tellman et al., 2021).

Contrary to traditionally ground-based observations or hydrological models, the launches of Gravity Recovery and Climate Experiment (GRACE) twin satellites in 2002 and its successor GRACE Follow-on (GRACE-FO) satellites in 2018 can provide a new methodology for retrieving terrestrial water storage anomalies (TWSA) in real time globally by measuring temporal variations in Earth's gravity field (Ahmed et al., 2021; Tapley et al., 2004). TWSA derived from GRACE/GRACE-
35 FO satellites comprises all the surface and subsurface water over land, which can be used to monitor the hydrologic variations in response to extreme weather events. In this case, GRACE/GRACE-FO observations have been widely applied to assess the potential flood risks for a specific region. For example, Reager et al. (2009) proposed a flood potential index estimated by using the monthly average precipitation anomalies and GRACE-derived TWSA to characterize the potential flood risks from regional to global scales. Xiong et al. (2021) developed a novel integrated flood potential index by linking
40 the flood potential index derived from six GRACE products based on a copula function, which was further used to identify and characterize the floods with different intensities over the study region. A summary of relevant literature on detecting extreme flood events using GRACE/GRACE-FO data has been listed in Table 1.

Previous studies have clearly indicated that the proposed indices using GRACE/GRACE-FO data can better reflect the evolution of flood events than traditional indices, such as standardized precipitation index (SPI) and standardized
45 precipitation evapotranspiration index (SPEI), because the GRACE/GRACE-FO observations can measure the vertically integrated water storage over regions (Yan et al., 2021; Yin et al., 2021). However, all these studies mainly focus on detecting the extreme flood events at monthly intervals while monitoring the flood events and its hydrological impacts at finer temporal scales remains a major challenge due to the coarse temporal resolution (i.e. monthly) of GRACE/GRACE-FO data. To date, very few studies have paid attention to monitor flood events at sub-monthly time scales using GRACE data.
50 Given the rapid occurrence and evolution of some extreme events within a short period, there is a great need to monitor the flood events at a finer temporal resolution (e.g. day), which has important implications for better understanding the mechanisms of extreme flood events in the Yangtze River Basin (YRB). Therefore, we aim to downscale the TWSA estimates derived from GRACE/GRACE-FO satellite data into daily values and demonstrate its application to monitor extreme flood events at sub-monthly time scales for the YRB. The temporally downscaled TWSA data could be valuable for
55 understanding the effects of climate change on the hydrological cycle and providing important implications of flood hazard prevention and water resource management over this region.

The YRB is one of the most important basins in China, because it can provide freshwater, hydropower, food, and other ecosystem services for hundreds of millions of people. Meanwhile, the YRB has been regarded as one of the most sensitive and vulnerable regions that suffered from severe floods due to its highly uneven rainfall pattern (Zhang et al., 2021). During
60 the past decades, the increasingly intensified human activities and climate change have substantially changed the

hydrological cycle in the YRB and thus accelerated the variation of flood characteristics in this region (Fang et al., 2012; Wang et al., 2011). It has been found that both the frequency and severity of extreme flood events generally showed an upward trend in the YRB in recent decades owing to substantial changes in climate, infrastructure and land use (Huang et al., 2015; Liu et al., 2019; Yang et al., 2021; Zhang et al., 2008). For example, in Year 2020, the YRB has experienced one of

65   the most extreme flood events on record. According to the data from the Ministry of Emergency Management of the People's Republic of China, a total of 38.173 million people were affected and 27,000 houses collapsed due to the 2020 flood, with 56 deaths or disappearances and a great economic loss of $27.68 billion (USD) (Jia et al., 2021).

The rest of this paper is mainly organized as follows. In Section 2, descriptions of the study area are presented. In Section 3 and Section 4, the datasets and methods used in this study are introduced respectively. In Section 5, monthly TWSA

70   estimates obtained from original GRACE/GRACE-FO satellite data are temporally downscaled into individual values at daily time scales based on the methodology proposed in this study. Meanwhile, a new index incorporating temporally downscaled TWSA estimates and daily precipitation is proposed to detect extreme flood events occurred in Year 2020 across the YRB and its individual subbasins. Then, the discussion about the temporally downscaled GRACE/GRACE-FO satellite data and its capacity to monitor extreme flood events are presented in Section 6. We also explain the reasons why the new

75   proposed index can monitor extreme flood events across the YRB in this section. Finally, we present a summary of this study in Section 7.

Table 1.

2 Study area

The Yangtze River (also termed as Changjiang River) is the longest river in China with a length of about 6,300 km. It

80   originates from the Tanggula Mountains of Qinghai-Tibetan Plateau and eventually empties into the estuary of the East China Sea after spanning over eleven provinces in China. The YRB (90°E - 122°E, 25°N - 35°N) has a total drainage area of 1.81 million km², which accounts for approximately 20% of the total area of the mainland China. The terrain of the YRB generally decreases from west to east with altitudes ranging from -142 m to 7143 m above the sea level (shown in Fig. 1). The entire YRB consists of three main parts, that is, the Upper (upstream region above the Yichang station), the Middle

85   (region between the Yichang station and the Hukou station) and the Lower (downstream region below the Hukou station) subbasins.

The YRB is located in typically subtropical and temperate climate zones, which is dominated by three types of monsoons, namely the Siberian northwest monsoon winds in winter, the Indian southeasterly monsoon winds and the East Asian monsoon in summer (Kong et al., 2020). According to the observations from meteorological stations, the mean annual air

90   temperature of this basin ranges from 14.4°C to 15.4°C and mean annual precipitation ranges from 1049 mm to 1424 mm

during 2003-2020. Under the joint effects of monsoon activities and seasonal motions of subtropical highs, more than 85% of the annual precipitation occurs in the wet season from April to October, which further increases the risks of extreme floods in the middle and lower reaches of the Yangtze River (Huang et al., 2015; Yang et al., 2010). Additionally, by the end of 21st century, projections show a significant upward trend of the annual precipitation over the YRB according to the latest study (Yue et al., 2021).

The YRB is one of the most important regions in China because it accommodates approximately 33% of China's total population (Huang et al., 2021), accounts for over 36% China's total water resources, and contributes more than 46% of China's total Gross Domestic Product (GDP) according to the statistics collected by Yangtze River Conservancy Commission of Ministry of Water Resources. The YRB not only sustains many hydro-electrical industries, such as the Three Gorges Corporation, but also provides freshwater resources for neighboring regions to alleviate the pressure of water scarcity through the South-to-North Water Diversion Project (Long et al., 2020; Zhang et al., 2021). Furthermore, the YRB can play a critical role in flood control, crop irrigation, power generation, and ecological conservation (Chao et al., 2021; Wang et al., 2020a). More information about the location and topography of the YRB can be found in Fig. 1.

Figure 1.

3 Data

3.1 Terrestrial water storage derived from GRACE/GRACE-FO satellite data

GRACE and GRACE-FO data can provide global TWSA at monthly scales. In this study, the average of three types of GRACE and GRACE-FO solutions is estimated in order to characterize the variations of TWSA in the YRB and its individual subbasins during the period of 2003-2020, all of which are the latest versions of Release Number 06 (RL06). These products are provided by the Center for Space Research (CSR, at the University of Texas at Austin) (Save et al., 2016), the Goddard Space Flight Center (GSFC, at NASA) (Loomis et al., 2019) and the Jet Propulsion Laboratory (JPL, at NASA and California Institute of Technology, California) (Landerer et al., 2020) respectively. All these GRACE and GRACE-FO solutions represented by equivalent water thickness units (mm) are anomalies relative to the time-mean baseline during January 2004 - December 2009. It should also be noteworthy that GRACE data in a few months are not available because of the problem of "battery management". In addition, there existed a gap period for 11 consecutive months from July 2017 to May 2018 between the GRACE and GRACE-FO satellites. Here we have not filled the data gaps between the two GRACE satellites with linear interpolation since it may not fully describe the seasonal variation of TWSA during these missing months. All these GRACE and GRACE-FO satellite data are available at the website of https://podaac.jpl.nasa.gov. As documented in previous studies (Long et al., 2014; Xie et al., 2022), there are slight differences between these three GRACE

120   and GRACE-FO solutions when estimating the variation of regional TWSA. The differences between these three GRACE and GRACE-FO solutions mainly arise from the processing algorithms or constrained solutions.

3.2 Meteorological data

In this study, daily time series of precipitation and temperature from 2003-2020 are provided by the China Meteorological Administration (CMA) (http://data.cma.cn/) with a total of 150 National Meteorological Observatory stations distributed in

125   the YRB (shown in Fig. 1). Areal precipitation in the YRB and its individual subbasins at daily scales can be calculated according to the Thiessen polygon method. Monthly precipitation for regions is calculated by summing all daily values of precipitation. Meanwhile, areal temperature in the YRB and its basins at daily time scales are calculated by directly averaging the respective daily temperature from all meteorological stations over regions. Similarly, monthly temperature estimates are calculated by summing all daily values of temperature.

130   ## 3.3 In-situ streamflow data

From the Yangtze River Conservancy Commission of Ministry of Water Resources, daily streamflow observations during the period of 2003-2020 can be obtained at the Shigu hydrological station, the Yichang hydrological station, the Hankou hydrological station and the Datong hydrological station (shown in Fig. 1). More specifically, the Shigu station represents the outlet of the Source regions of the Yangtze River Basin (SYRB), the Yichang station represents the outlet of the Upper

135   regions of the Yangtze River Basin (UYRB), the Hankou station represents the outlet of the Upper and the Middle regions of the Yangtze River Basin (UMYRB), and the Datong station represents the outlet of the entire Yangtze River Basin (YRB). Meanwhile, extreme flood events in the YRB and its individual subbasins during the study period can be extracted from daily time series of streamflow observed from the above hydrological stations (Tarasova et al., 2018). More details about how the extreme flood events are extracted will be described in the Section 4.4.

140   ## 3.4 Soil moisture storage

As documented in Xie et al. (2019a), soil moisture storage (SMS), as one of critical components of terrestrial water storage, usually shows a significantly positive correlation with variations of regional TWSA. Therefore, in this study we adopt the SMS (kg/m^2) with a spatial resolution of $0.25° \times 0.25°$ from the Global Land Data Assimilation System version 2.1 (GLDAS 2.1) Noah land surface model to estimate their correlations with regional TWSA derived from the GRACE and GRACE-FO

145   satellite data. This product can provide the simulations of SMS at four different depths of soil layers from 0 to 200 cm, that is, 0 - 10 cm, 10 - 40 cm, 40 - 100 cm and 100 - 200 cm depths per three hours. To keep consistent with TWSA, the original value of SMS should be transferred into soil moisture storage anomaly values (SMSA) after subtracting the time-mean baseline during the period of 2004-2009. Furthermore, the temporal resolution of original SMS derived from GLDAS 2.1

Noah land surface model can be decreased from 3-hours to 1-day and 1-month composite respectively, which is consistent with the methods applied in previous studies (Mulder et al., 2015; Mohanasundaram et al., 2021; Syed et al., 2008).

Table 2.

4 Methods

To better monitor the extreme flood events occurred in the YRB, monthly TWSA obtained from original GRACE/GRACE-FO satellite data are temporally downscaled into individual values at daily time scales based on the methodology proposed in this study. A detailed flow diagram of our study is given in Fig. 2, which consists of four steps. In Step 1, meteorological observations including precipitation, temperature provided by CMA and SMSA derived from the GLDAS 2.1 Noah land surface model are jointly used as model inputs to establish the relationship with detrended GRACE/GRACE-FO satellite data. In Step 2, the relationship between TWSA estimates and all hydro-climatic factors at monthly time scales for the YRB can be built by using three different machine learning-based models, namely MLP model, LSTM model and MLR model respectively. Given that different periods of data used for training and validation might influence the performances of each model in simulating TWSA, a total of three scenarios are therefore designed according to the way of dividing training periods and validation periods for each model. After comparing the performances of each model in simulating monthly TWSA estimates under all three scenarios, the calibrated parameter sets of the model with a specific scenario that shows the best performance in simulating monthly TWSA estimates are identified and retained. In Step 3, daily time series of meteorological observations and the SMSA from the GLDAS 2.1 Noah land surface model are reselected as model inputs of the relationship established in Step 2 assuming that scaling properties at the monthly time scales are valid at the daily time scales. And hence daily TWSA estimates can be temporally downscaled from monthly TWSA estimates by using the calibrated model parameter sets that have been identified. In Step 4, daily time series of TWSA are further applied to monitor the flood events at sub-monthly time scales for different basins in the YRB according to the new proposed index.

Figure 2.

Specifically, three types of models, namely, the artificial neural network (ANN), the recurrent neural network (RNN) and the multiple linear regression (MLR) are used as the statistical downscaling methods. In order to keep a fair comparison, we will choose identical inputs and outputs in the process of training these three models. Furthermore, the GRACE satellite can provide TWSA estimates under the joint effects of human activities and climatic variability (Xie et al., 2019b). As pointed out by previous studies (Humphrey and Gudmundsson, 2019; Khorrami et al., 2021; Shah et al., 2021), long-term changes in TWSA are primarily caused by frequent human activities such as persistent groundwater overexploitation and massive construction of large reservoirs. For example, the YRB is a typical region strongly influenced by various human activities, such as the construction of Three Gorges Reservoir and intense human water consumption (Huang et al., 2015; Yao et al.,

2021). In this study, the linear trends have been removed from the original time series of TWSA in the training and calibration periods because hydro-climatic factors may not fully simulate these long-term trends, all of which are mainly arising from human activities, such as the water withdrawals and reservoir operation over the study region (Rodell et al., 2018). More detailed descriptions about the methods used in this study are given as follows.

4.1 Multi-layer perceptron neural network (MLP)

The ANN is a black box model which has the ability to imitate the thought processes of the human brain and thus can be applied to deal with complex and nonlinear problems (Bomers et al., 2019; Boucher et al., 2020; Lecun et al., 2015; Wang et al., 2020b). Among different types of ANNs, the multi-layer perceptron neural network (MLP) with the Levenberg-Marquardt Back Propagation training algorithm is the most widely used method as it requires relatively less time in the process of convergence (Rumelhart et al., 1986; Xie et al., 2019a). Therefore, a three-layer MLP model and the Logarithmic Sigmoid as a transfer function are jointly used for temporal downscaling in this study, which has been proved to be effective and reliable in statistical downscaling (Nourani et al., 2018; Sharifi et al., 2019). This MLP model consists of three parts, namely, an input layer, a hidden layer and an output layer, all of which finally form a network through many neurons. Meanwhile, the weights, which are connections between different neurons, can adjust as learning proceeds until the most optimum network is derived in this process (Fig. 3(a)).

In this study, the variables included in the input layer are precipitation, temperature and SMS whereas the variable included in the output layer is detrended TWSA. Based on trial-by-error, the most optimal number of hidden neurons is set to five. After minimizing the discrepancy between the simulated TWSA with the observed results at the output layer, the most optimal network architecture can be finally obtained.

4.2 Long short-term memory network (LSTM)

The recurrent neural network (RNN) (Rumelhart et al., 1986) is a unique type of deep learning algorithm that was developed to process sequential data and predict future trends. One of the most dominated features of the RNN layer is a unique feedback connection which can allow past information to continuously affect the current output. The characteristics of all related time series data can be eventually learned through this structure. Long short-term memory network (LSTM) is one of the most representative RNNs as it has the fabulous memory ability and can effectively avoid the vanishing gradient problem existing in other RNNs (Hochreiter, 1997; Guo et al., 2021). Considering the time series characteristics of meteorological data and TWSA data, the LSTM model can be very suitable as a statistical downscaling model for its excellent capacity to process sequence-to-sequence learning problems.

One typical LSTM model usually consists of three layers, that is, an input layer, a hidden layer and an output layer (Fig. 3(b)). Different from other traditional ANNs, the LSTM model replaces the hidden block in RNNs with a memory cell state

coupled with three logic gates, that is, the forget gate, the input gate and the output gate. In the training process, the memory cell state mainly stores the accumulation of past information. The input gate determines how much information of a new input flows into the memory cell state at the current time. Then, the useless information in long-term memory would be forgotten by the forget gate, which determines how much of the former moment is retained to the current time. Finally, the output gate determines how much information of the memory cell state is used to compute output (Bai et al., 2021; Wu et al., 2020; Vu et al., 2021).

Figure 3.

4.3 Multiple linear regression (MLR)

The multiple linear regression (MLR) is a typical statistical approach that can be applied to establish the relationships between inputs and outputs (Sousa et al., 2007). This approach has a wide range of hydrological applications since it can well explain the linkage between various variables (Lyu et al., 2021; Ramesh et al., 2020; Sun et al., 2020). Here we assume that the GRACE/GRACE-FO derived TWSA is linearly regressed onto the meteorological variables (i.e. precipitation and temperature) and the SMS obtained from GLDAS 2.1 simultaneously, that is:

$$y = \sum_{i=1}^{3} a_i \times x_i + b, \tag{1}$$

where y represents TWSA at monthly (or daily) scales; x_i ($i = 3$) represents three independent inputs including precipitation, temperature and SMS at monthly (or daily) scales; a_i represents the corresponding regression coefficients of each input, which can be calculated by the least-squares regression method; b represents a constant offset.

4.4 Flood event selection

A nonparametric algorithm suggested by Tarasova et al. (2018) is adopted to identify runoff events in this study, which has been widely applied in many different basins over the world because of its advantages in identifying flood events (Fischer et al., 2021; Giani et al., 2022; Lu et al., 2020; Winter et al., 2022). A brief procedure of this algorithm is described as follows: (1) picking out local minima within nonoverlapping five-day windows with respect to the entire streamflow time series; (2) examining the extracted series of minima with the goal of finding turning points, all of which are usually defined as the points that are at least 1.11 times smaller than their neighboring minima; (3) reconstructing the base flow hydrograph according to the linear interpolation between the turning points, which are previously obtained in Step (2); (4) screening the streamflow time series to identify runoff events after the separation of base flow. Traditionally, a typical runoff event can be characterized by three main components, namely peak, beginning, and end points. A peak refers to the maximum of streamflow for a specific period. The beginning point refers to the closest point in time when total runoff is equal to base

flow before the peak. Similarly, the end point denotes the closest point in time when total runoff is equal to base flow after the peak.

4.5 Daily flood potential index

240   The flood potential index provides a surrogate measure of the potential flood risks for a specific region, which can be obtained from monthly average precipitation anomalies and GRACE-derived TWSA (Reager et al., 2009). In this study, we further propose a new normalized daily flood potential index (NDFPI) with reference to Reager et al. (2009) and Abhishek et al. (2021). Compared to the original flood potential index, the NDFPI can not only provide useful information on the early signs of the region's transition from normal state to a flood-prone situation but also effectively detect the flood events at sub-

245   monthly time scales, which is calculated via the following steps:

$$TWSA_{def}(t) = TWSA_{max} - TWSA(t-1), \tag{2}$$

where $TWSA_{def}(t)$ (mm) represents the terrestrial water storage deficit for a specific day (t) that is defined as the difference between the historic storage anomaly time series maximum during the entire period ($TWSA_{max}$) and the storage amount from the previous day ($TWSA$ (t-1)).

250   Then, the daily flood potential amount (DFPA) is further calculated as follows:

$$DFPA(t) = P(t) - TWSA_{def}(t) = P(t) - (TWSA_{max} - TWSA(t-1)), \tag{3}$$

where $DFPA(t)$ (mm) represents the daily flood potential amount for a specific day (t); $P(t)$ (mm) represents the daily precipitation; $TWSA(t$-1) (mm) represents the TWSA from the previous day (t-1).

Finally, we can calculate the normalized daily flood potential index (NDFPI) from the DFPA with the goal of removing the

255   effects of hydrological heterogeneity varying from region to region and the typical difference between the storage change and precipitation that may not always result in floods (Reager et al., 2009), which can be described as follows:

$$NDFPI(t) = \frac{DFPA(t) - DFPA_{min}}{DFPA_{max} - DFPA_{min}}, \tag{4}$$

where $DFPA_{max}$ and $DFPA_{min}$ represent the maximum DFPA and minimum DFPA during the study period respectively. The NDFPI indicates the corresponding probability of flood occurrence with a range from 0 to 1. More flood is likely to

260   occur when the NDFPI is closer to 1 for a specific region.

4.6 Model test design

Monthly TWSA estimates during the extreme flood events occurred in the YRB can be reconstructed at regional scales based on the above three different learning-based models, namely the MLP model, the LSTM model and the MLR model.

Meanwhile, these three models are further validated in four different basins covering from the upstream to downstream of the Yangtze River in order to better evaluate their applications. More detailed information about all these four different basins can also refer to Table S1. According to previous findings in Liu et al. (2021), different periods of data used for training (i.e. identification of model parameter sets) and validation can eventually influence the corresponding performances of a specific model when simulating TWSA. Therefore, we design a total of three scenarios according to the way of dividing training periods and validation periods for a specific model. As shown in Fig. 2, periods of GRACE data used for training and validation in each experiment are listed, which include (1) Scenario 1: training period (2003/01-2014/07, a total of 129 months) and validation period (2014/08-2020/12, a total of 56 months), (2) Scenario 2: training period (2005/06-2018/06, a total of 129 months) and validation period (2003/01-2005/05 and 2018/07-2020/12, a total of 56 months), and (3) Scenario 3: training period (2007/10-2020/12, a total of 129 months) and validation period (2003/01-2007/09, a total of 56 months). Furthermore, three kinds of statistical measures including root mean square error (RMSE), correlation coefficient (r), and Nash-Sutcliffe efficiency coefficient (NSE) are used in this study as they can jointly measure the matching quality in terms of both magnitude and phase between the simulated and the observed time series. These statistical measures are defined as:

$$RMSE = \sqrt{\frac{\sum_{i=1}^{N}(x_{s,i}-x_{o,i})^2}{N}}, \tag{5}$$

$$r = \frac{\sum_{i=1}^{N}(x_{s,i}-\bar{x}_{s,i})(x_{o,i}-\bar{x}_{o,i})}{\sqrt{\sum_{i=1}^{N}(x_{s,i}-\bar{x}_{s,i})^2 \times \sum_{i=1}^{N}(x_{o,i}-\bar{x}_{o,i})^2}}, \tag{6}$$

$$NSE = 1 - \frac{\sum_{i=1}^{N}(x_{s,i}-x_{o,i})^2}{\sum_{i=1}^{N}(x_{o,i}-\bar{x}_{o,i})^2}, \tag{7}$$

where $x_{s,i}$ and $x_{o,i}$ represent simulated and observed TWSA in month i, respectively; $\bar{x}_{s,i}$ and $\bar{x}_{o,i}$ represent the average of simulated and observed TWSA series; N is the total months of observed (or simulated) TWSA available.

5 Results

5.1 Temporal variation of precipitation, temperature, SMSA, TWSA and streamflow across the YRB during 2003-2020

Fig. 4 shows the monthly time series of SMSA, TWSA, streamflow and the main climatic variables including precipitation and temperature across the YRB during 2003-2020.The results show that monthly TWSA over the YRB has a wide range from -58.0 mm to 130.9 mm during the study period. Monthly TWSA estimated by three GRACE/GRACE-FO solutions changes synchronously with precipitation across the entire YRB, showing a significantly positive correlation between TWSA and precipitation ($r = 0.54$; $p < 0.01$) during the study period. According to the statistics collected by Yangtze River

Conservancy Commission of Ministry of Water Resources, the accumulative rainfall across the entire YRB exceeds 680 mm in summer 2020 from April to October, which is far more than the mean rainfall (approximately 540 mm) during the same period from 2003 to 2019. Accordingly, TWSA reaches its maximum in July 2020 with an estimate of 130.9 mm during 2003-2020, reflecting the evolution of TWSA in response to heavy rainfall during this period. In addition to precipitation, TWSA is also highly consistent with temperature over the YRB during 2003-2020, showing a positive correlation coefficient of $r = 0.57$ ($p < 0.01$) with monthly temperature.

The GLDAS Noah-derived SMSA and GRACE/GRACE-FO derived TWSA both show a seasonal variation through the entire study period in the YRB, but there exists a significant difference in the intensity of anomalies between them especially in the summer season as depicted in Fig. 4. This phenomenon can be explained by the discrepancies resulting from the components of SMSA and TWSA. Although the SMSA is an important component of TWSA for many regions, the latter usually contains some other components, such as the anomalies of surface water and groundwater etc., besides the SMSA (Xie et al., 2021). There exists a significant correlation between TWSA and SMSA with a positive correlation coefficient of $r = 0.84$ ($p < 0.01$), both of which reach to maximum and minimum values almost simultaneously. In general, TWSA shows a significant correlation with precipitation, temperature and SMSA during the study period, all of which have been therefore selected as the inputs applied to simulate monthly TWSA over different regions.

Figure 4.

5.2 Reconstruction of TWSA by different models

To achieve the temporal downscaling of monthly TWSA data and fill the missing months for TWSA, we should firstly build the relationships between GRACE/GRACE-FO derived TWSA and various hydro-climatic factors including precipitation, temperature and SMSA at monthly time scales. The results of TWSA are estimated by the mean value in different regions upstream of the corresponding hydrological stations shown in Fig. 1. In this study, three different models including MLP, LSTM and MLR are adopted to reconstruct TWSA for regions. Table 3 shows the summary of model performances in reconstructing monthly TWSA across the YRB during the study period. GRACE/GRACE-FO satellite data used for training (i.e. identification of model parameter sets) and validation shown in each scenario mainly depend on the periods of series of data as suggested by Liu et al. (2021). According to Table 3, we find that all models including the MLP, the LSTM and the MLR with Scenario 3 show the best performances in simulating monthly TWSA under all three designed scenarios. This result indicates that the models with Scenario 3 is relatively superior to the models with the other two scenarios when simulating TWSA because the data in Scenario 3 contains more extremely high (or low) values during the study period in the process of training models. Therefore, in the following sections, we decide to directly divide the training periods and validation periods of all these models according to Scenario 3 (shown in Table 3) when simulating monthly TWSA for other regions besides the YRB.

Table 3.

Fig. 5 show the comparison between monthly TWSA derived from GRCACE/GRACE-FO satellite data and that simulated by different models for all regions during 2003-2020. The corresponding evaluation values are also presented in this figure. We find that the maximum NSEs between the GRACE/GRACE-FO-derived TWSA estimates and that simulated by models are 0.68, (Fig. 5(a)), 0.82 (Fig. 5(f)), 0.86 (Fig. 5(g)) and 0.89 (Fig. 5(j)) during the validation periods for the SYRB, the UYRB, the UMYRB and the YRB, respectively. The corresponding RMSEs are 13.2 mm/month, 13.7 mm/month, 12.4 mm/month and 10.9 mm/month (validation periods, hereafter) for the SYRB, the UYRB, the UMYRB and the YRB, respectively. In general, the detrended TWSA estimates present consistent values between the observations and the modeled results from 2003-2020 for most regions except for the SYRB, as shown in Fig. 5. Compared to the other regions, all models show a relatively poor performance in simulating monthly TWSA for the SYRB with NSEs less than 0.70 during the validation periods, which can be mainly attributed to the increased uncertainties in precipitation and temperature induced by the sparse distribution of meteorological stations over this region (shown in Fig. 1).

We further compare separately the performances of all models in simulating monthly TWSA for a specific region. Taking the entire YRB as an example (Fig. 5(j-l)), GRACE/GRACE-FO derived TWSA estimates show a RMSE of 10.9 mm/month for the MLP-derived TWSA estimates, which is lower than that of 15.1 mm/month for the LSTM-derived TWSA estimates (~39% difference) and that of 13.3 mm/month for the MLR-derived TWSA estimates (~22% difference). Meanwhile, the NSE shows similar improvements when applying the MLP model to simulate TWSA for the YRB (Fig. 5(j-l)), which can also be found in the SYRB (Fig. 5(a-c)) and the UMYRB (Fig. 5(g-i)). In general, the MLP and MLR models achieve high metrics (0.81/12.8 mm/month and 0.75/14.2 mm/month of NSE/RMSE on average for all regions) during the validation periods, both of which are significantly higher than the metrics between the GRACE/GRACE-FO derived TWSA estimates and that simulated by the LSTM model (0.75/14.7mm of NSE/RMSE on average for all regions). For the UYRB (Fig. 5(d-f)), the MLP model shows a slightly poor performance in simulating TWSA in terms of a higher RMSE (14.7 mm/month) than the LSTM model (14.5 mm/month; ~1.2% increase) and the MLR model (13.7 mm/month; ~7.2% increase). In addition, it seems that the larger the study region, the higher the correspondence between the GRACE/GRACE-FO derived TWSA estimates and that simulated by models for the MLP model. This result can be explained that the large area for a specific region may smooth more uncertainties in GRACE signals and meteorological observations (Long et al., 2015).

Overall, Fig. 5 clearly suggests the MLP model's superior performances in simulating TWSA with an average value of NSE of 0.81 and an average value of RMSE of 12.8 mm/month during the validation periods for all regions, showing the outstanding capability of MLP model in learning the complicated relationships between TWSA and hydro-climatic factors. As documented in Shu et al. (2007), the MLP model can show its unique superiority and great advantages compared with other statistical models particularly when explaining the underlying processes that have complex nonlinear interrelationships. The results shown in Fig. 5 also indicate that the MLP model can show a relatively better performance in simulating monthly

TWSA than the LSTM model in this study. As described in Zhang et al. (2018), one of main drawbacks of the LSTM model is its complexity compared with the MLP model, which indicates that the LSTM model may not show better performances in

355   simulating time series data than other traditional ANN models in some cases especially when limited trained data are available. In addition, the moderate performance of LSTM model in reconstructing TWSA compared to the MLP model can be partly attributed to the possibly limited role of the memory function in the LSTM model (Wei et al., 2021; Yin et al., 2022), since relations between inputs and the output of this model (shown in Figure 4) are pretty direct without much memory effects. Therefore, in the following discussion, only the MLP model is applied to further achieve the temporal

360   downscaling of monthly TWSA data for regions.

Figure 5.

5.3 Temporal downscaling of GRACE/GRACE-FO satellite data

Relationships between monthly TWSA and hydro-climatic inputs with respect to the entire YRB have been fully established as presented in Section 5.2. As documented in Herath et al. (2016) and Requena et al. (2021), the same scaling properties

365   have been commonly assumed for baseline and future periods in temporal downscaling. Therefore, it is reasonable and acceptable to assume that scaling properties at the monthly time scales are valid at the daily time scales in this study (Kumar et al., 2012). That is, the relationship between temporally downscaled TWSA and daily hydro-climatic inputs is consistent with that previously established by the downscaling model (e.g. the MLP model) at monthly time scales for a specific region. By merging the daily hydro-climatic inputs into the previously established relationships between TWSA estimates and

370   hydro-climatic factors based on the MLP model, we can downscale the TWSA estimates from monthly time series to daily time series for all regions.

Fig. 6 shows daily time series of TWSA temporally downscaled by the MLP model for different regions during 2003-2020. It can be seen that daily TWSA shows sub-monthly signals in response to changes in hydro-climatic factors as expected. Both GRACE/GRACE-FO derived TWSA estimates and daily TWSA estimates temporally downscaled by the MLP model

375   show obvious seasonal cycles and reach to their respective extreme values almost simultaneously. More specific, amplitudes of daily TWSA estimates are slightly higher (or lower) than monthly TWSA estimates in summer (or winter) seasons from 2003 to 2020. This can be deemed as reasonable because monthly TWSA estimates are defined as the mean average of daily TWSA estimates for a specific month. It should also be noted that there still exist some discrepancies between temporally downscaled TWSA at sub-monthly time scales and monthly TWSA estimates derived from GRACE/GRACE-FO satellite

380   data for the SYRB particularly in some extreme low values, which can be attributed to the relatively poor relationship between TWSA estimates and hydro-climatic factors for this region as described in Fig. 5(a). As documented in previous studies (Liu et al., 2020; Shi et al., 2020), it has long been challenging to accurately perform hydrological simulation across the SYRB because of the complex hydrological processes for this alpine basin. For example, parameter settings calibrated by

GLDAS Noah land surface model might not be highly accurate for SMS simulation across the SYRB, because field measurements of SMS in this region are extremely limited. Harsh climatic conditions and limited weather stations can additionally influence the accuracy of meteorological observations such as precipitation and temperature across the SYRB especially for some extreme values. Given the above reasons, there is a relatively poor relationship between TWSA estimates and hydro-climatic factors across the SYRB based on the MLP (shown in Fig. 5(a)). Furthermore, the uncertainty in the observed precipitation and temperature and SMS derived from the GLDAS Noah land surface model can eventually result in some discrepancies between temporally downscaled TWSA at sub-monthly time scales and monthly TWSA estimates derived from GRACE/GRACE-FO satellite data, as described in Fig. 6(a).

Figure 6.

5.4 Relation between daily TWSA and streamflow during flood events

Fig. 7 and Fig. 8 show the daily TWSA temporally downscaled by the MLP model and observed streamflow within the YRB in 2010 and 2020 when extreme flood events occurred according to the information published by the Yangtze River Conservancy Commission of Ministry of Water Resources. As described in Fig. 7 and Fig. 8, the nonparametric simple smoothing method introduced in Section 4.4 can effectively identify the corresponding flood events occurred in each region based solely on the analysis of streamflow time series. It shows an apparent increase in streamflow from the beginning to peak of all flood events. Accordingly, the daily TWSA shows a distinct increase similar with streamflow during the same periods as expected. It is also interesting to note that the beginning of increase shown in daily TWSA is earlier than that of streamflow. This is partly because high antecedent soil moisture, which is an important component of TWSA, has been identified as an important driver of flood events for regions (Fatolazadeh et al., 2022; Jing et al., 2020; Reager et al., 2014; Wasko et al., 2019). Meanwhile, this result indicates that daily TWSA can be potentially useful in building early flood warning systems since it may identify the extreme flood events much more earlier than streamflow.

Figure 7.

Figure 8.

5.5 Monitoring severe flood events based on the proposed NDFPI in Year 2020

To better monitor severe flood events over the YRB, we propose a new index, i.e. NDFPI, by jointly using the temporally downscaled TWSA data and daily precipitation data as introduced in Section 4.5. According to the Yangtze River Conservancy Commission of Ministry of Water Resources, the YRB has suffered from catastrophic flooding in Year 2020. Therefore, in this study, the severe flood events occurred in 2020 for the YRB will be served as an example to present the capability of NDFPI in detecting extreme flood events. The threshold values of daily streamflow and NDFPI for the 90th percentile floods during 2003-2020 are presented in Fig. 9. According to the results shown in Fig. 9, the larger threshold

values of NDFPI usually indicate severity of flood occurrences increases for a specific region. In addition, the shape of percentile duration curve of daily streamflow across the UYRB (Fig. 9(b)) is different with that shown in other regions. It is noted that the outlet of the UYRB, the Yichang hydrological station, is located approximately 45 km downstream of the Three Gorges Reservoir (shown in Fig. 1), which is one of the largest hydroelectric reservoirs in the world. Given that the operations of the Three Gorges Reservoir can directly affect the streamflow at Yichang station (Yang et al., 2022), the result shown in Fig. 9(b) is reasonable.

Figure 9.

Fig. 10 shows the comparison between basin averaged NDFPI and daily streamflow observations for the 90th percentile floods in 2020. The results indicate that the ups and downs of the streamflow observed at different hydrological stations are highly consistent with the NDPFI results through the whole season. For example, the observations of streamflow from the Shigu hydrological station (Fig. 10(a)) reached its 90th percentile in July 12. In comparison, the NDFPI estimated by temporally downscaled TWSA and daily precipitation reached its 90th percentile in July 4 (Fig. 10 (a)), which is nine days earlier than that of daily streamflow. As expected, these high streamflow observations during the wet season are usually accompanied by high NDPFI values, which could be attributed to the effects of high precipitation on streamflow during this period. For the YRB (Fig. 10 (d)), daily streamflow detected at the Datong hydrological station reached its 90th percentile in June 29 and eventually peaked in July 13 with a maximum value of 7.2×10^9 m^3/day, which is in line with the findings in Jia et al. (2021). Accordingly, the series of NDFPI reached its 90th percentile in June 18 with a value of 0.58. In general, Fig. 10 clearly suggests that the proposed NDFPI calculated by temporally downscaled TWSA data and daily precipitation changes synchronously with the reality of flood disasters in 2020 for the YRB. Meanwhile, it also indicates that such flood events can be monitored by the proposed NDFPI earlier than traditional streamflow observations.

Figure 10.

Previous studies usually focus on monitoring the long-term flood events while the flood events at sub-monthly time scales using GRACE/GRACE-FO satellite data have been limitedly investigated due to the limitation of its temporal resolution (i.e. month) (Gouweleeuw et al., 2018; Long et al., 2014). In this study, however, Fig. 10 clearly shows the incremental process of TWSA during the wet season using the new proposed NDFPI estimated by temporally downscaled GRACE/GRACE-FO satellite data and daily precipitation for different regions. This means that the proposed NDFPI has the great potential to detect the evolution of extreme flood events within the short period. It is also interesting to note that the NDFPI reached the threshold of different classes of flood events earlier than that defined by streamflow observations during the wet season in 2020, which can be repeatedly found in the SYRB, the UYRB, the UMYRB and the YRB (Fig. 10) respectively. The comparison results indicate that the lag time between the threshold values of flood events monitored by the NDFPI and that monitored by daily streamflow during the wet season ranges from 8 to 15 days for the 90th percentile floods among all regions in 2020, all of which are far less than the temporal resolution of original GRACE/GRACE-FO satellite data (i.e.

month). In addition to the 90th percentile floods, we also compare the basin averaged NDFPI and daily streamflow observations for the 95th and 99th percentile floods in 2020 (shown in Supplement Figure S1-S4). The results also show that the series of NDFPI reached the threshold values earlier than that of daily streamflow observations for the 95th and 99th percentile floods. For example, there exists a 11-day lag time between the threshold value of NDFPI and that of the

450 streamflow observed by Datong hydrological station for the 99th percentile floods in 2020 (Fig. S4(d)), which provides useful information for accurate and timely flood forecasts and can be very beneficial for protecting people and infrastructure over regions in a changing climate.

6 Discussion

6.1 Extreme flood events monitored by NDFPI

455 The comparison results indicate that the proposed NDFPI reached the threshold values of different classes of flood events earlier than that defined by streamflow observations in 2020 with respect to the YRB and its individual subbasins (shown in Figure 8 and Figure S1-S4). This is consistent with the results found at the Missouri River basin by Reager et al. (2014). Reager et al. (2014) indicated that regional TWSA may lead river discharge slightly before the flood season, which can provide useful information on the signal of high streamflow in the coming flood season. However, the study of Reager et al

460 (2014) only demonstrated the application of GRACE data to characterize regional flood potential at monthly time scales. More accurate information about the complete hydrologic state of a specific region at sub-monthly time scales during the wet season has been limitedly investigated, which is very vital for flood warnings. Given this in mind, we proposed a new index, i.e. NDFPI, by jointly using the temporally downscaled TWSA data and daily precipitation data to better analyze the hydrologic state of the study region during the wet season at finer time scales.

465 The comparison analysis of the NDFPI and daily streamflow with respect to the YRB may explain the possible reasons why the NDFPI can detect extreme flood events for a specific river basin. Intense rainfall of long duration can cause continuous increases in the surface water (e.g. water stored in lakes and wetlands), soil moisture storage and groundwater storage that are totally represented by TWSA in this study through the process of infiltration. Many studies also revealed that changes in surface water, soil moisture and groundwater under intense rainfall can exert obvious effects on the status of regional TWSA

470 (Döll et al., 2012; Felfelani et al., 2017; Sinha et al., 2019; Velicogna et al., 2012). All these changes may ultimately result in the saturation of aquifer over regions. However, the saturated state of aquifers is not persistent because there is a great need for the basin to relieve its saturated state by discharging excessive water stored on and below the land surface into the river channels, which may eventually lead to the dramatic increase in streamflow and greatly increase the risk of widespread and damaging regional flooding.

6.2 Advantages of detecting extreme flood events based on temporally downscaled TWSA

The traditional flood monitoring approaches mainly provide useful information about the evolution of flood events over the study region through the measurements of rainfall and streamflow. All these measurements largely depend on the in-situ hydrological stations and rainfall gauging stations distributed over the regions, which are difficult to achieve in some regions with harsh environment and climatic conditions. In comparison, satellite remote sensing has no such limitation of traditional point-based observations, making it a promising approach to monitor extreme flood events particularly in some poorly gauged basins. Given the large spatial extent, complicated climatic condition, and inaccessible hydrological observations for some high-altitude regions (e.g. SYRB), GRACE TWSA has shown great advantages and superiority in flood monitoring and water resources management for the YRB than traditional flood monitoring approaches.

Furthermore, all these traditional flood monitoring approaches mainly focus on the meteorological conditions or the status of surface water reflecting by various hydro-climatic factors and pay little attention to the importance of antecedent terrestrial water storage conditions before flood events, which can play a critical role in capturing the flood formation processes (Xiong et al., 2021). For example, Reager et al. (2009) applied the TWSA from GRACE data and monthly precipitation to assess the likelihood for flooding at the regional scale and emphasized the importance of terrestrial water storage signal in the accurate prediction of floods and general runoff. Long et al. (2014) employed the index of flood potential amount using GRACE data and monthly precipitation to investigate hydrological floods and droughts for a large karst plateau in Southwest China and found that higher TWSA estimates are more prone to result in large potential for flooding during rainy season because of the excessive water that cannot be stored further. Therefore, the new proposed index incorporating TWSA can more holistically quantify the potential of the development of severe floods for regions than common flood potential indices using hydro-climatic observations.

While previous studies have proposed several standardized indices for large-scale flood monitoring based on GRACE-derived TWSA (Chen et al., 2010; Tangdamrongsub et al., 2016), flood monitoring and assessment at sub-monthly time scales remains a challenge using GRACE data due to its coarse temporal resolution (month). Flood monitoring at finer time scales is pivotal in understanding the regional water cycle under climate change, which ultimately helps to manage the basin-scale water resources effectively and improve the efficiency of early flood warning systems. The application of daily series of TWSA temporally downscaled from GRACE/GRACE-FO satellite data can provide a useful method to comprehensively assess the integrated flood condition considering the changes of both surface and subsurface water storage at sub-monthly time scales. The highest difference in the temporally downscaled TWSA and the daily precipitation during the wet season, as revealed by the NDFPI, can indicate the early signs of the region's transition from normal state to a flood-prone situation. Overall, the new proposed NDFPI is proven to be a useful tool for flood monitoring with the finer time scale over large-scale basins, which also makes it possible to monitor extreme flood events timely especially for some regions with limited in-situ streamflow observations.

6.3 Uncertainties and limitations

By using the method of linear detrending, long-term trends in series of TWSA estimates have been removed during the reconstruction of TWSA, because they are generally driven by various human activities such as irrigation, reservoir operation and water withdrawals, all of which cannot be well reconstructed by hydro-climatic factors (Humphrey and Gudmundsson, 2019). Although the detrending method can reduce the impacts of human activities on reconstructing TWSA to some degree, it could still result in some discrepancies between the results of detrended TWSA and natural TWSA under climatic variability particularly in some regions where intense human activities existed. In future, more attentions should be paid to reconstruct the series of regional TWSA under climatic variability when more detailed statistics related to human use such as water consumption, reservoir operation and inter-basin water diversion projects are available. Meanwhile, TWSA estimates in some months are not available for the GRACE and GRACE-FO satellite due to the problem of "battery management". Although all these missing months can be effectively filled by different machine-learning based models, it may overestimate or underestimate the actual TWSA especially for some extreme values in the peak of the wet or dry season (Abhishek et al., 2022).

Furthermore, this study presents an effective way to temporally downscale the TWSA estimates from monthly time series into daily values. This temporal downscaling method is assessed through four case studies across the entire YRB, which could well present the temporal evolution of TWSA at sub-monthly time scales during the wet season. As this study mainly focus on characterizing regional flood potential based on the new proposed NDFPI incorporating temporally downscaled TWSA estimates, we applied this temporal downscaling method on the basin scale. In theory, this method is also suitable for the temporal downscaling of GRACE/GRACE-FO satellite data at the grid cell scale. However, as pointed out by previous studies (Landerer et al., 2012; Save et al., 2016; Scanlon et al., 2016), gridded TWSA estimates derived from GRACE/GRACE-FO satellite data involve relatively large uncertainty induced by associated measurement errors and signal leakage errors. As a result, the accuracy of TWSA estimates can ultimately exert a direct influence on the optimized parameter sets that are obtained for trained models in each grid cell, which is a contributing factor of the uncertainty. In addition, the forcing data of these models used for temporal downscaling, including air temperature, precipitation and GLDAS Noah derived SMSA, may also contain some errors and uncertainties due to the uneven spatial distribution of meteorological stations and natural measurement errors (Lv et al., 2017). These errors and uncertainties from the input data could be propagated into the machine learning-based models (e.g. MLP model), resulting in a broad range of differences between the observations and the simulated results. The latest study has made some initial attempts to learn the spatio-temporal patterns of difference between TWSA derived from GRACE data and those simulated by land surface models based on the convolutional neural network (CNN) models with the goal of providing more accurate TWSA estimates (Mo et al., 2022; Sun et al., 2019). Therefore, a thorough consideration of the spatio-temporal patterns of difference between TWSA derived from GRACE/GRACE-FO satellite data and those simulated by other hydrological models will be further taken in

our future work when downscaling the TWSA estimates in order to better understand the complex underlying mechanism for

540   TWSA variations during the wet season. Additionally, more efforts should be made to further validate the reliability of temporally downscaled relations proposed in this study when more independent data sources (e.g. groundwater level measurements) are available in YRB.

Overall, the present study shows the great potential of temporally downscaled GRACE/GRACE-FO satellite data in a wide range of hydrological applications, such as monitoring the extreme flood events. The study provides an effective means for

545   the temporal downscaling of original TWSA estimates from GRACE/GRACE-FO satellite data and will help facilitate the sustainable management of water resources and develop monitoring and early warning systems for severe flood events over large-scale basins. The methods and results shown in this study can provide important implications of flood hazard prevention and water resource management for other similar basins that are prone to suffer from severe extreme floods. Furthermore, this study can also provide broader implications for flood monitoring in ungauged or poorly gauged basins. For

550   example, advances in satellite remote sensing have made remote sensing a promising approach to capture various hydrological variables (e.g. precipitation, temperature and soil moisture) (Table S2), since they can substantially reduce the limitations of traditional ground-based observations. This is extremely useful and important in hydrological research and applications particularly in ungauged or poorly gauged basins. Therefore, we can calculate the flood potential index proposed in this study (i.e. NDFPI) by jointly using remote sensing-based precipitation, temperature and soil moisture

555   estimates combined with GRACE/GRACE-FO satellite data, which can further provide the potential of remote sensing data for flooding in ungauged or poorly gauged basins.

7 Conclusions

In the present study, we downscaled the GRACE/GRACE-FO derived TWSA estimates from monthly time series to daily time series in the YRB by establishing a relationship between TWSA estimates and hydro-climatic factors based on machine

560   learning techniques. Furthermore, the temporally downscaled TWSA data combined with daily precipitation were adopted to monitor the extreme flood events over the entire YRB in 2020 based on a new daily flood potential index. The main conclusions can be drawn as follows:

(1) When reconstructing monthly TWSA in the YRB, the MLP model shows the best performance with RMSE = 10.9 mm/month, NSE = 0.89, the MLR model follows with RMSE =13.4 mm/month, NSE = 0.84, and the LSTM model shows

565   the lowest performance with RMSE = 15.1 mm/month, NSE = 0.81 during the validation period;

(2) Based on the MLP model, monthly time series of TWSA were temporally downscaled to daily estimates by using meteorological observations and the outputs from a land surface model. The results show highly consistency with original monthly TWSA estimates derived from GRACE/GRACE-FO satellite data with regard to seasonal cycles;

(3) By jointly using daily average precipitation anomalies and temporally downscaled TWSA, the proposed NDFPI can

570 effectively detect the flood events at sub-monthly time scales occurred in 2020 for the entire YRB;

(4) The comparison analysis indicates that different types of flood events including the 90th, 95th and 99th percentile floods can be monitored by the proposed NDFPI earlier than traditional streamflow observations with respect to the YRB and its individual subbasins, which is very vital for flood forecasts and warning across this region.

Author Contributions

575 Yue-Ping Xu and Jingkai Xie designed the study; Yue-Ping Xu guided the research and revised the manuscript; Jingkai Xie did the main calculations and wrote the draft of the manuscript; Hongjie Yu and Yan Huang performed data pre-processing; Yuxue Guo helped to process the raw GRACE data.

Code/Data availability

The authors would like to thank both China Meteorological Administration and Yangtze River Conservancy Commission of
580 Ministry of Water Resources (http://www.cjw.gov.cn/) for providing the meteorological observations and hydrological data used in this study. We sincerely thank the NASA MEaSUREs Program and the Center for Space Research for providing GRACE/GRACE Follow-On JPL and CSR Level 3 Release 6 data, both of which are available from https://podaac.jpl.nasa.gov. We also sincerely thank the Goddard Earth Sciences (GES) Data and Information Services Center (DISC) for providing soil moisture storage acquired from the Global Land Data Assimilation System (GLDAS) data
585 (https://disc.sci.gsfc.nasa.gov/).

Acknowledgements

This study is financially sponsored by the National Natural Science Foundation of China (52109037, 52009121), Zhejiang Key Research and Development Program (2021C03017), and the Fundamental Research Funds for the Zhejiang Provincial Universities (2021XZZX015).

590 **Competing interests**

The authors declare that they have no conflict of interest.

References

Abhishek., Kinouchi, T., Abolafia-Rosenzweig, R., Ito, M., 2022. Water Budget Closure in the Upper Chao Phraya River Basin, Thailand Using Multisource Data. Remote Sens. 14(1), 173.

595 Abhishek., Kinouchi, T., Sayama, T., 2021. A comprehensive assessment of water storage dynamics and hydroclimatic extremes in the Chao Phraya River Basin during 2002-2020. J. Hydrol. 603, 126868.

Ahmed, M., Aqnouy, M., Messari, J.S.E., 2021. Sustainability of Morocco's groundwater resources in response to natural and anthropogenic forces. J. Hydrol. 603, 126866.

Bai, P., Liu, X., Xie, J., 2021. Simulating runoff under changing climatic conditions: A comparison of the long short-term

600 memory network with two conceptual hydrologic models. J. Hydrol. 592, 125779.

Bomers, A., van der Meulen, B., Schielen, R.M.J., Hulscher, S.J.M.H., 2019. Historic flood reconstruction with the use of an Artificial Neural Network. Water Resour. Res. 55, 9673-9688.

Boucher, M.A., Quilty, J., Adamowski, J., 2020. Data assimilation for streamflow forecasting using extreme learning machines and multilayer perceptrons. Water Resour. Res. 56, e2019WR026226.

605 Chao, N., Jin, T., Cai, Z., Chen, G., Liu, X., Wang, Z., Yeh, P.J.F., 2021. Estimation of component contributions to total terrestrial water storage change in the Yangtze river basin. J. Hydrol. 595, 125661.

Chen, J.L., Wilson, C.R., Tapley, B.D., 2010. The 2009 exceptional Amazon flood and interannual terrestrial water storage change observed by GRACE. Water Resour. Res. 46, W12526.

Chen, X., Jiang, J., Li, H., 2018. Drought and flood monitoring of the Liao River Basin in northeast China using extended

610 GRACE Data. Remote Sens. 10(8), 1168.

Dottori, F., Szewczyk, W., Ciscar, J., Zhao, F., Alfieri, L., Hirabayashi, Y., Bianchi, A., Mongelli, I., Frieler, K., Betts, R.A., Feyen, L., 2018. Increased human and economic losses from river flooding with anthropogenic warming. Nat. Clim. Change. 8, 781-786.

Döll, P., Hoffmann-Dobrev, H., Portmann, F.T., Siebert, S., Eicker, A., Rodell, M., Strassberg, G., Scanlon, B.R., 2012.

615 Impact of water withdrawals from groundwater and surface water on continental water storage variations. J. Geodyn. 59-60, 143-156.

Fang, H., Han, D., He, G., Chen, M., 2012. Flood management selections for the Yangtze River midstream after the Three Gorges Project operation. J. Hydrol. 432-433, 1-11.

Fatolazadeh, F., Goïta, Kalifa., 2022. Reconstructing groundwater storage variations from GRACE observations using a new

620 Gaussian-Han-Fan (GHF) smoothing approach. J. Hydrol. 604, 127234.

Felfelani, F., Wada, Y., Longuevergne, L., Pokhrel, Y.N., 2017. Natural and human-induced terrestrial water storage change: A global analysis using hydrological models and GRACE. J. Hydrol. 553, 105-118.

Fischer, S., Schumann, A., Bühler, P., 2021. A statistics-based automated flood event separation. J. Hydrol. X, 10, 100070.

Giani, G., Tarasova, L., Woods, R.A., Rico-Ramirez, M.A., 2022. An objective time-series-analysis method for rainfall-runoff event identification. Water Resour. Res. 58, e2021WR031283.

Gouweleeuw, B.T., Kvas, A., Gruber, C., Gain, A.K., Mayer-Gürr, T., Flechtner, F., Güntner, A., 2018. Daily GRACE gravity field solutions track major flood events in the Ganges-Brahmaputra Delta. Hydrol. Earth Syst. Sci. 22, 2867-2880. https://doi.org/10.5194/hess-22-2867-2018.

Guo, Y., Yu, X., Xu, Y.P., Chen, H., Gu, H., Xie, J., 2021. AI-based techniques for multi-step streamflow forecasts: application for multi-objective reservoir operation optimization and performance assessment. Hydrol. Earth Syst. Sci., 25, 5951-5979.

Herath, S.M., Sarukkalige, P.R., Nguyen, V.T.V., 2016. A spatial temporal downscaling approach to development of IDF relations for Perth airport region in the context of climate change. Hydrol. Sci. J. Des Sci. Hydrol. 61, 2061-2070.

Hochreiter, S., Schmidhuber, J., 1997. Long short-term memory. Neural Comput. 9 (8), 1735-1780.

Huang, S., Zhang, X., Chen, N., Li, B., Ma, H., Xu, L., Li, R., Niyogi, D., 2021. Drought propagation modification after the construction of the Three Gorges Dam in the Yangtze River Basin. J. Hydrol. 603, 127138.

Huang, Y., Salama, M.S., Krol, M.S., Su, Z., Hoekstra, A.Y., Zeng, Y., Zhou, Y., 2015. Estimation of human-induced changes in terrestrial water storage through integration of GRACE satellite detection and hydrological modeling: A case study of the Yangtze River basin. Water Resour. Res. 51 (10), 8494-8516.

Humphrey, V., Gudmundsson, L., 2019. GRACE-REC: a reconstruction of climate-driven water storage changes over the last century. Earth Syst. Sci. Data 11 (3), 1153-1170.

Jia, H., Chen, F., Pan, D., Du, E., Wang, L., Wang, N., Yang, A., 2021. Flood risk management in the Yangtze River basin - Comparison of 1998 and 2020 events. Int. J. Disaster Risk Reduct. 68, 102724.

Jing, W., Di, L., Zhao, X., Yao, L., Xia, X., Liu, Y., Yang, J.i., Li, Y., Zhou, C., 2020. A data-driven approach to generate past GRACE-like terrestrial water storage solution by calibrating the land surface model simulations. Adv. Water Resour. Res. 143, 103683.

Khorrami, B., Gunduz, O., 2021. An enhanced water storage deficit index (EWSDI) for drought detection using GRACE gravity estimates. J. Hydrol. 603, 126812.

Kong, R., Zhang, Z., Zhang, F., Tian, J., Chang, J., Jiang, S., Zhu, B., Chen, X., 2020. Increasing carbon storage in subtropical forests over the Yangtze River basin and its relations to the major ecological projects. Sci. Total Environ. 709, 136163.

Kumar, J., Brooks, B.-G.J., Thornton, P.E., Dietze, M.C., 2012. Sub-daily statistical downscaling of meteorological variables using neural networks. Proc. Comput. Sci. 9, 887-896. http://dx.doi.org/10.1016/j.procs. 2012.04.095

Landerer, F. W., Flechtner, F. M., Save, H., Webb, F. H., Bandikova, T., Bertiger, W. I., et al., 2020. Extending the global mass change data record: GRACE Follow-On instrument and science data performance. Geophys. Res. Lett. 47(12), e2020GL088306.

Landerer, F.W., Swenson, S.C., 2012. Accuracy of scaled GRACE terrestrial water storage estimates. Water Resour. Res. 48 (4), W04531.

LeCun, Y., Bengio, Y., Hinton, G., 2015. Deep learning. Nature 521 (7553), 436-444.

Liu, B., Zou, X., Yi, S., Sneeuw, N., Cai, J., Li, J., 2021. Identifying and separating climate- and human-driven water storage anomalies using GRACE satellite data. Remote Sens. Environ. 263, 112559.

Liu, L., Jiang, L., Wang, H., Ding, X., Xu, H., 2020. Estimation of glacier mass loss and its contribution to river runoff in the source region of the Yangtze River during 2000-2018. J. Hydrol. 589, 125207.

Liu, X.J., Min, F.Y., Kettner, A.J., 2019. The impact of large to extreme flood events on floodplain evolution of the middle and lower reaches of the Yangtze River, China. Catena 176, 394-409.

Long, D., Shen, Y., Sun, A., Hong, Y., Longuevergne, L., Yang, Y., Li, B., Chen, L., 2014. Drought and flood monitoring for a large karst plateau in Southwest China using extended GRACE data. Remote Sens. Environ. 155, 145-160.

Long, D., Yang, W., Scanlon, B.R., Zhao, J., Liu, D., Burek, P., Pan, Y., You, L., Wada, Y., 2020. South-to-North Water Diversion stabilizing Beijing's groundwater levels. Nat. Commun. 11, 3665. https://doi.org/10.1038/s41467-020-17428-6.

Long, D., Yang, Y., Wada, Y., Hong, Y., Liang, W., Chen, Y., Yong, B., Hou, A., Wei, J., Chen, L., 2015. Deriving scaling factors using a global hydrological model to restore GRACE total water storage changes for China's Yangtze River Basin. Remote Sens. Environ. 168, 177-193.

Long, D., Shen, Y., Sun, A., Hong, Y., Longuevergne, L., Yang, Y., Li, B., Chen, L., 2014. Drought and flood monitoring for a large karst plateau in Southwest China using extended GRACE data. Remote Sens. Environ. 155, 145-160.

Loomis, B.D., Luthcke, S.B. Sabaka, T.J., 2019. Regularization and error characterization of GRACE mascons. J. Geodesy. 93, 1381-1398.

Lu, W., Lei, H., Yang, W., Yang, J., Yang, D., 2020. Comparison of Floods Driven by Tropical Cyclones and Monsoons in the Southeastern Coastal Region of China. J. Hydrometeorol. 21(7), 1589-1603.

Lv, M., Ma, Z., Yuan, X., Lv, M., Li, M., Zheng, Z., 2017. Water budget closure based on GRACE measurements and reconstructed evapotranspiration using GLDAS and water use data for two large densely-populated mid-latitude basins. J. Hydrol. 547, 585-599.

Lyu, K., Zhang, X., Church, J.A., 2021. Projected ocean warming constrained by the ocean observational record. Nat. Clim. Change. 11, 834-839.

685   Mulder, G., Olsthoorn, T.N., Al-Manmi, D.A.M.A., Schrama, E.J.O., Smidt, E.H., 2015. Identifying water mass depletion in northern Iraq observed by GRACE. Hydrol. Earth Syst. Sci. 19 (3), 1487-1500.

Mohanasundaram, S., Mekonen, M.M., Haacker, E., Ray, C., Lim, S., Shrestha, S., 2021. An application of GRACE mission datasets for streamflow and baseflow estimation in the Conterminous United States basins. J. Hydrol. 601, 126622.

Mo, S., Zhong, Y., Forootan, E., Mehrnegar, N., Yin, X., Wu, J., Feng, W., Shi, X., 2022. Bayesian convolutional neural
690   networks for predicting the terrestrial water storage anomalies during GRACE and GRACE-FO gap. J. Hydrol. 604, 127244.

Nourani, V., Baghanam, A.H., Gokcekus, H., 2018. Data-driven ensemble model to statistically downscale rainfall using nonlinear predictor screening approach. J. Hydrol. 565, 538-551.

Ramesh, K., Smith, A.K., Garcia, R.R., Marsh, D.R., Sridharan, S., Kumar, K.K., 2020. Long-term variability and
695   tendencies in middle atmosphere temperature and zonal wind from WACCM6 simulations during 1850-2014. J. Geophys. Res. Atmos. 125(24), e2020JD033579.

Reager, J.T., Famiglietti, J.S., 2009. Global terrestrial water storage capacity and flood potential using GRACE. Geophys. Res. Lett. 36, L23402. https://doi.org/10.1029/2009GL040826.

Reager, J.T., Thomas, B.F., Famiglietti, J.S., 2014. River basin flood potential inferred using GRACE gravity observations at
700   several months lead time. Nat. Geosci. 7 (8), 588-592. https://doi.org/10.1038/ngeo2203.

Requena, A.I., Nguyen, T.H., Burn, D.H., Coulibaly, P., 2021. A temporal downscaling approach for sub-daily gridded extreme rainfall intensity estimation under climate change. J. Hydrol. Reg. Stud. 35, 100811.

Rodell, M., Famiglietti, J.S., Wiese, D.N., Reager, J.T., Beaudoing, H.K., Landerer, F.W., Lo, M.H., 2018. Emerging trends in global freshwater availability. Nature 557, 6510659.

705   Rumelhart, D.E., Hinton, G.E., Williams, R.J., 1986. Learning representations by backpropagating errors. Nature 323, 533-536.

Save, H., Bettadpur, S., Tapley, B.D., 2016. High-resolution CSR GRACE RL05 mascons. J. Geophys. Res. Solid Earth. 121, 7547-7569.

Scanlon, B.R., Zhang, Z., Save, H., Wiese, D.N., Landerer, F.W., Long, D., Longuevergne, L., Chen, J.L., 2016. Global
710   evaluation of new GRACE mascon products for hydrologic applications. Water Resour. Res. 52 (12), 9412-9429.

Shah, D., Mishra, V., 2021. Strong influence of changes in terrestrial water storage on flood potential in India. J. Geophys. Res. Atmos. 126, e2020JD033566.

Sharifi, E., Saghafian, B., Steinacker, R., 2019. Downscaling satellite precipitation estimates with multiple linear regression, artificial neural networks, and spline interpolation techniques. J. Geophys. Res. Atmos. 124, 789-805.

715   Shi, R., Yang, H., Yang, D., 2020. Spatiotemporal variations in frozen ground and their impacts on hydrological components in the source region of the Yangtze River. J. Hydrol. 590, 125237.

Shu, C., Ouarda, T.B., 2007. Flood frequency analysis at ungauged sites using artificial neural networks in canonical correlation analysis physiographic space. Water Resour. Res. 43, W07438.

Sinha, D., Syed, T.H., Reager, J.T., 2019. Utilizing combined deviations of precipitation and GRACE-based terrestrial water storage as a metric for drought characterization: A case study over major Indian river basins. J. Hydrol. 572, 294-307.

Slater, L.J., Villarini, G., 2016. Recent trends in U.S. flood risk. Geophys. Res. Lett. 43, 12428-12436.

Sousa, S.I.V., Martins, F.G., Alvim-Ferraz, M.C.M., Pereira, M.C., 2007. Multiple linear regression and artificial neural networks based on principal components to predict ozone concentrations. Environ. Modell. Software 22 (1), 97-103.

Sun, A.Y., Scanlon, B.R., Zhang, Z., Walling, D., Bhanja, S.N., Mukherjee, A., Zhong, Z., 2019. Combining physically based modeling and deep learning for fusing GRACE satellite data: can we learn from mismatch? Water Resour. Res. 55 (2), 1179-1195.

Sun, Z., Long, D., Yang, W., Li, X., Pan, Y., 2020. Reconstruction of GRACE data on changes in total water storage over the global land surface and 60 basins. Water Resour. Res. 56(4), e2019WR026250.

Syed, T.H., Famiglietti, J.S., Rodell, M., Chen, J., Wilson, C.R., 2008. Analysis of Terrestrial Water Storage Changes from GRACE and GLDAS. Water Resour. Res. 44, W02433.

Tangdamrongsub, N., Ditmar, P.G., Steele-Dunne, S.C., Gunter, B.C., Sutanudjaja, E.H., 2016. Assessing total water storage and identifying flood events over Tonlé Sap basin in Cambodia using GRACE and MODIS satellite observations combined with hydrological models. Remote Sens. Environ. 181, 162-173.

Tanoue, M., Taguchi, R., Nakata, S., Watanabe, S., Fujimori, S., Hirabayashi, Y., 2020. Estimation of direct and indirect economic losses caused by a flood with long-lasting inundation: Application to the 2011 Thailand flood. Water Resour. Res. 56, e2019WR026092.

Tapley, B.D., Bettadpur, S., Ries, J.C., Thompson, P.F., Watkins, M.M., 2004. GRACE measurements of mass variability in the earth system. Science 305, 503. https://doi.org/10.1126/science.1099192.

Tarasova, L., Basso, S., Zink, M., Merz, R., 2018. Exploring controls on rainfall-runoff events: 1. Time series-based event separation and temporal dynamics of event runoff response in Germany. Water Resour. Res. 54, 7711-7732.

Tellman, B., Sullivan, J.A., Kuhn, C., Kettner, A.J., Doyle, C.S., Brakenridge, G.R., Erickson, T.A., Slayback, D.A., 2021. Satellite imaging reveals increased proportion of population exposed to floods. Nature 596, 80-86.

Velicogna, I., Tong, J., Zhang, T., Kimball, J.S., 2012. Increasing subsurface water storage in discontinuous permafrost areas of the Lena River basin, Eurasia, detected from GRACE. Geophys. Res. Lett. 39(9), L09403.

Vu, M,T., Jarhani, A., Massei, N., Fournier, M., 2021. Reconstruction of missing groundwater level data by using Long Short-Term Memory (LSTM) deep neural network. J. Hydrol. 597, 125776.

Wang, L., Chen, C., Na, X., Fu, Z., Zheng, Y., Peng, Z., 2020a. Evaluation of GRACE mascon solutions using in-situ geodetic data: The case of hydrologic-induced crust displacement in the Yangtze River Basin. Sci. Total Environ. 707, 135606.

750 Wang, M., Zheng, H., Xie, X., Fan, D., Yang, S., Zhao, Q., Wang, K., 2011. A 600-year flood history in the Yangtze River drainage: comparison between a subaqueous delta and historical records. Chin. Sci. Bull. 58 (2), 188-195.

Wang, Q., Huang, J., Liu, R., Men, C., Guo, L., Miao, Y., Jiao, L., Wang, Y., Shoaib, M., Xia, X., 2020b. Sequence-based statistical downscaling and its application to hydrologic simulations based on machine learning and big data. J. Hydrol. 586, 124875.

755 Wasko, C., Natthan, R., 2019. Influence of changes in rainfall and soil moisture on trends in flooding. J. Hydrol. 575, 432-441.

Wei, L., Jiang, S., Ren, L., Tan, H., Ta, W., Liu, Y., Yang, X., Zhang, L., Duan, Z., 2021. Spatiotemporal changes of terrestrial water storage and possible causes in the closed Qaidam Basin, China using GRACE and GRACE Follow-On data. J. Hydrol. 598, 126274.

760 Winter, C., Tarasova, L., Lutz, S.R., Musolff, A., Kumar, R., Fleckenstein, J.H., 2022. Explaining the Variability in High-Frequency Nitrate Export Patterns Using Long-Term Hydrological Event Classification. Water Resour. Res. 58, e2021WR030938.

Wu, H., Yang, Q., Liu, J., Wang, G., 2020. A spatiotemporal deep fusion model for merging satellite and gauge precipitation in China. J. Hydrol. 584, 124664.

765 Xie, J., Xu, Y.P., Wang, Y., Gu, H., Wang, F., Pan, S., 2019a. Influences of climatic variability and human activities on terrestrial water storage variations across the Yellow River basin in the recent decade. J. Hydrol. 579, 124218.

Xie, J., Xu, Y.P., Gao, C., Xuan, W., Bai, Z., 2019b. Total basin discharge from GRACE and Water balance method for the Yarlung Tsangpo River basin, Southwestern China. J. Geophys. Res. Atmos. 124, 7617-7632.

Xie, J., Xu, Y.P., Guo, Y., Wang, Y., 2021. Detecting the dominant contributions of runoff variance across the source region
770 of the Yellow River using a new decomposition framework. Hydrol. Res. 52(5), 1015-1032.

Xie, J., Xu, Y., Guo, Y., Wang, Y., Chen, H., 2022. Understanding the impact of climatic variability on terrestrial water storage in the Qinghai-Tibet Plateau of China. Hydrolog. Sci. J. 67(6), 1-16.

Xiong, J., Guo, S., Yin, J., 2021. Discharge Estimation Using Integrated Satellite Data and Hybrid Model in the Midstream Yangtze River. Remote Sens. 13, 2272.

775 Xiong, J., Yin, J., Guo, S., Gu, L., Xiong, F., Li, N., 2021. Integrated flood potential index for flood monitoring in the GRACE era. J. Hydrol. 603, 127115.

Yan, X., Zhang, B., Yao, Y., Yang, Y., Li, J., Ran, Q., 2021. GRACE and land surface models reveal severe drought in eastern China in 2019. J. Hydrol. 601, 126640.

Yang, S., Liu, Z., Dai, S., Gao, Z., Zhang, J., Wang, H., Luo, X., Wu, C., Zhang, Z., 2010. Temporal variations in water resources in the yangtze river (Changjiang) over the industrial period based on reconstruction of missing monthly discharges. Water Resour. Res. 46, W10516.

Yang, P., Xia, J., Luo, X., Meng, L., Zhang, S., Cai, W., Wang, W., 2021. Impacts of climate change-related flood events in the Yangtze River Basin based on multi-source data. Atmos. Res. 263, 105819.

Yang, L., Zeng, S., Xia, J., Wang, Y., Huang, R., Chen, M., 2022. Effects of the Three Gorges Dam on the downstream streamflow based on a large-scale hydrological and hydrodynamics coupled model. J Hydrol Reg Stud 40, 101039.

Yao, L., Li, Y., Chen, X., 2021. A robust water-food-land nexus optimization model for sustainable agricultural development in the Yangtze River Basin. Agric. Water Manag. 256, 107103.

Yin, G., Park, J., 2021. The use of triple collocation approach to merge satellite- and model-based terrestrial water storage for flood potential analysis. J. Hydrol. 603, 127197.

Yin, H., Wang, F., Zhang, X., Zhang, Y., Chen, J., Xia, R., Jin, J., 2022. Rainfall-runoff modeling using long short-term memory based step-sequence framework. J. Hydrol. 610, 127901.

Yue, Y., Yan, D., Yue, Q., Ji, G., Wang, Z., 2021. Future changes in precipitation and temperature over the Yangtze River Basin in China based on CMIP6 GCMs. Atmos. Res. 264, 105828.

Zhang, D., Lindholm, G., Ratnaweera, H., 2018. Use long short-term memory to enhance Internet of Things for combined sewer overflow monitoring. J. Hydrol. 556, 409-418.

Zhang, Q., Xu, C.Y., Zhang, Z.X., Chen, Y.D., Liu, C.L., Lin, H., 2008. Spatial and temporal variability of precipitation maxima during 1960-2005 in the Yangtze River basin and possible association with large-scale circulation. J. Hydrol. 353 (3-4), 215-227.

Zhang, X., Zhang, G., Long, X., Zhang, Q., Liu, D., Wu, H., Li, S., 2021. Identifying the drivers of water yield ecosystem service: A case study in the Yangtze River Basin, China. J. Hydrol. 132, 108304.

Table 1: A summary of relevant literature on monitoring extreme flood events using GRACE/GRACE-FO data. GRACE = Gravity Recovery and Climate Experiment mission; GRACE-FO = Gravity Recovery and Climate Experiment Follow-On mission; GLDAS = Global Land Data Assimilation system; TRMM = Tropical Rainfall Measuring Mission; MODIS = Moderate-Resolution Imaging Spectroradiometer.

Study	Study region	Source data	Period	Temporal resolution	Main contributions
Chen et al. (2010)	Amazon basin	GRACE RL04 data; precipitation	2002 to 2009	Month	Measuring large-scale extreme flood events
Long et al. (2014)	Yun-Gui Plateau	GRACE RL05 data; hydrometeorological data	2003 to 2012	Month	Evaluating the frequency and severity of droughts and floods over the regions
Reager et al. (2014)	Mississippi River basin	GRACE data; GLDAS data; stream gauge data	2003 to 2011	Month	Characterizing regional flood potential and assessing the predisposition of a river basin to flooding
Tangdamrongsub et al. (2016)	Tonlé Sap basin	GRACE RL05 data; TRMM; MODIS; hydrological model	2002 to 2014	Month	Quantifying the flood events at both basin and sub-basin scales
Chen et al. (2018)	Liao River basin	GRACE RL05 data; meteorological data; hydrological model	2002 to 2016	Month	Monitoring the drought and flood patterns based on the total storage deficit index
Yang et al. (2021)	Yangtze River Basin	GRACE/GRACE-FO RL06 data; meteorological data; teleconnection indices	2002 to 2018	Month	Investigating the flood risk factors and analyzing the impact of climate change factors on flood events
Shah et al. (2021)	Indian subcontinent	GRACE RL06 data; meteorological data	2002 to 2016	Month	Examining the role of changes in terrestrial water and groundwater storage on flood potential
This study	Yangtze River	GRACE/GRACE-FO	2003 to	Day	Monitoring the evolution of

Basin	RL06 data; runoff; meteorological data	2020		extreme flood events based on temporally downscaled GRACE data

Table 2: An overview of all datasets used in this study.

Data	Source	Temporal resolution	Spatial resolution	Time span
Terrestrial water storage anomaly (TWSA)	GRACE/GRACE-FO CSR	Month	0.5°	2002 - 2020
	GRACE/GRACE-FO JPL	Month	0.5°	2002 - 2020
	GRACE/GRACE-FO GSFC	Month	0.5°	2002 - 2020
Soil moisture storage (SMS)	GLDAS 2.1 - Noah	3 hours	1°	2002 - 2020
Precipitation (P)	CMA	Day	/	2003 - 2020
Temperature (T)	CMA	Day	/	2003 - 2020
Streamflow	In situ	Day	/	2003 - 2020

Note. GRACE = Gravity Recovery and Climate Experiment mission; GRACE-FO = Gravity Recovery and Climate Experiment Follow-On mission; CSR = Center for Space Research; JPL = Jet Propulsion Laboratory; GSFC = Goddard Space Flight Center; GLDAS = Global Land Data Assimilation system; CMA = China Meteorological Administration.

Table 3: Performances of different models in simulating monthly TWSA across the YRB during 2003-2020.

Scenarios		MLP (RMSE/NSE)	LSTM (RMSE/NSE)	MLR (RMSE/NSE)
Scenario 1	2003/01 - 2014/06 (Training) (70%)	10.71/0.89	12.14/0.86	11.63/0.87
	2014/08 - 2020/12 (Validation) (30%)	26.12/0.50	26.62/0.15	24.32/0.57
Scenario 2	2005/06 - 2018/06 (Training) (70%)	13.54/0.84	14.61/0.79	14.33/0.82
	2003/01 - 2005/05 and 2018/07 - 2020/12 (Validation) (30%)	23.32/0.59	25.42/0.17	20.14/0.70
Scenario 3	2007/10 - 2020/12 (Training) (70%)	15.76/0.80	17.84/0.68	17.24/0.76
	2003/01 - 2007/09 (Validation) (30%)	10.92/0.89	15.12/0.81	13.41/0.84

Note. TWSA = Terrestrial water storage anomalies; YRB = Yangtze River Basin; MLP = Multi-layer perceptron neural network; LSTM = Long short-term memory network; MLR = Multiple linear regression. 70%, 30% and 100% represent the corresponding proportions to all samples in the training, the validation and the entire periods respectively. RMSE/NSE represent the Root mean square error (mm/month) and Nash-Sutcliffe efficiency coefficient between the simulated TWSA with the observed TWSA respectively. Noted that GRACE/GRACE-FO derived TWSA in some months are not available due to the problem of battery management.
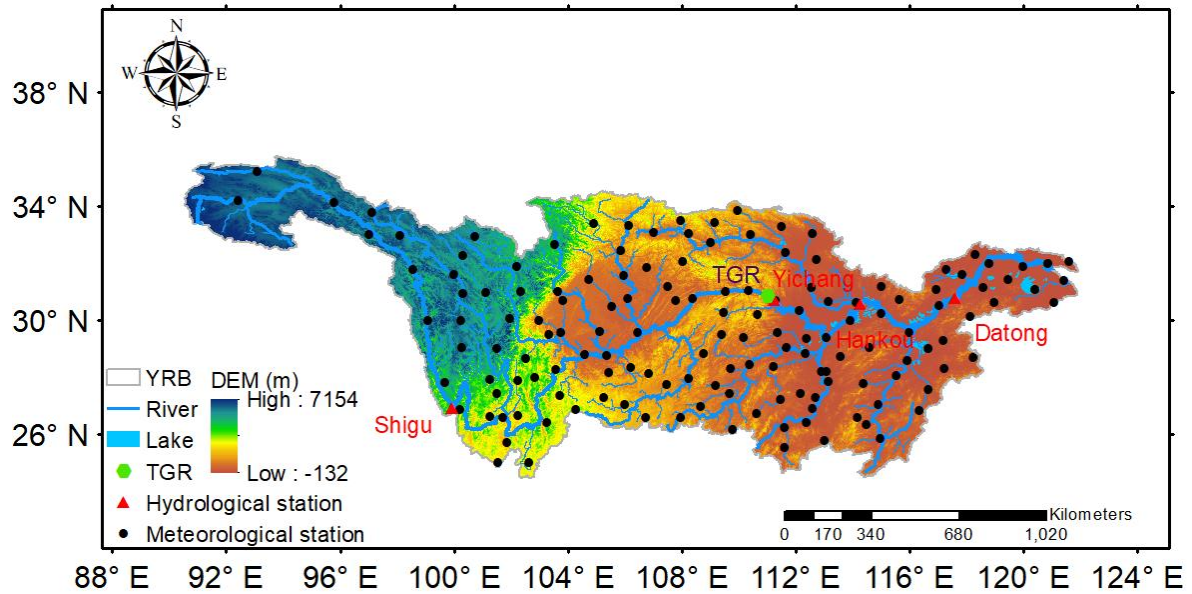
Figure 1: Location of the Yangtze River Basin (YRB) in China and its topography. Distribution of meteorological stations and hydrological stations are also shown in this figure. TGR = Three Gorges Reservoir; DEM = Digital Elevation Model.

820
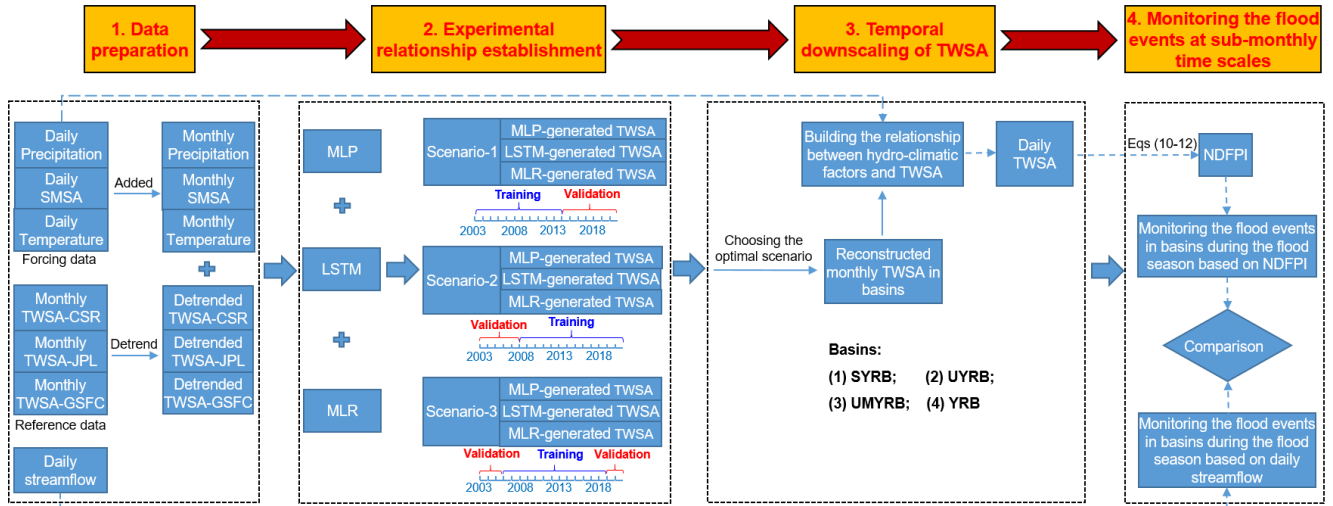
Figure 2: A detailed flow diagram illustrating the temporal downscaling of GRACE/GRACE-FO derived TWSA. GRACE = Gravity Recovery and Climate Experiment mission; GRACE-FO = Gravity Recovery and Climate Experiment Follow-On mission; SMSA = Soil moisture storage anomaly; TWSA = Terrestrial water storage anomaly; CSR = Center for Space Research; JPL = Jet Propulsion Laboratory; GSFC = Goddard Space Flight Center; SYRB = Source regions of the Yangtze River Basin; UYRB = Upper regions of the Yangtze River Basin; UMYRB = Upper and the Middle regions of the Yangtze River Basin; YRB = Yangtze River Basin; MLP = Multi-layer perceptron neural network; LSTM= Long short-term memory; MLR = Multiple linear regression; NDFPI = Normalized daily flood potential index.

825
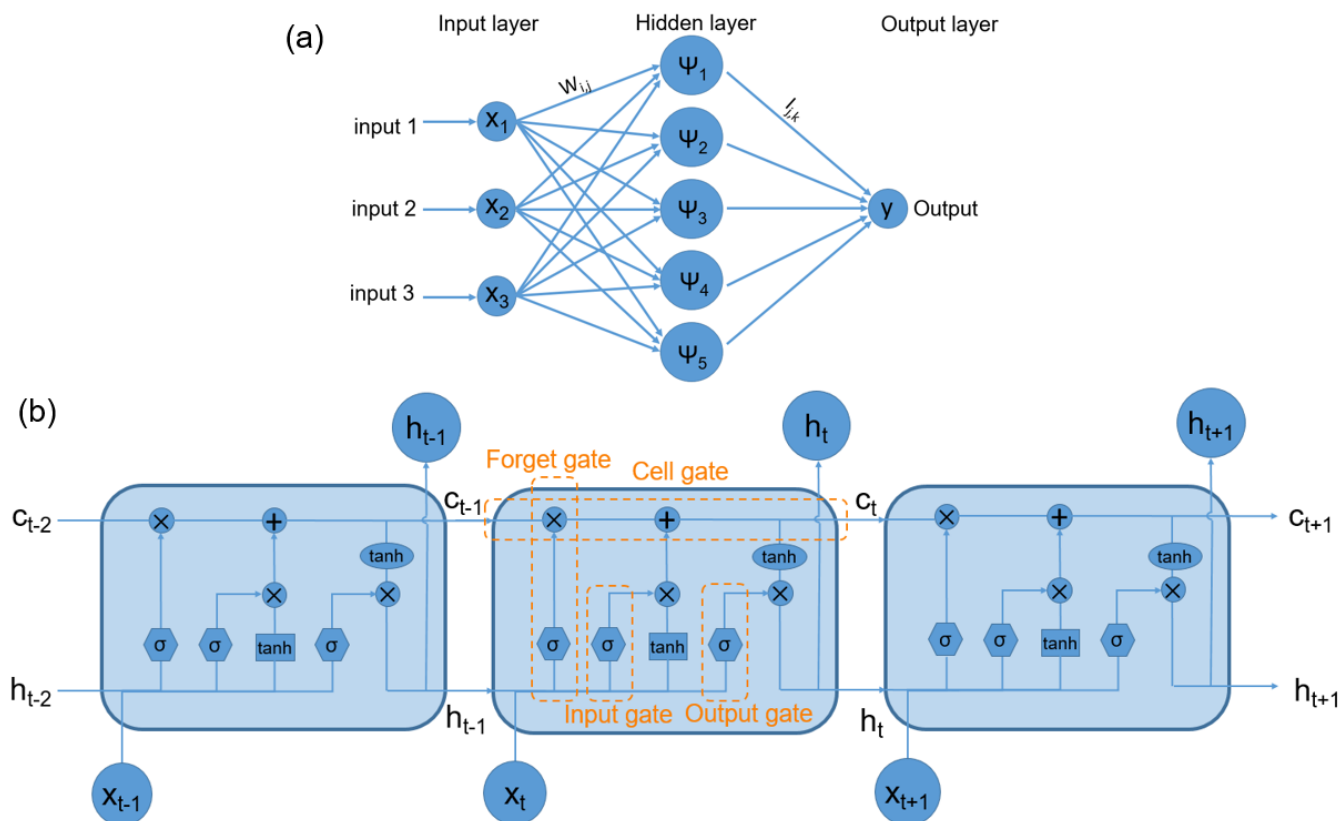
Figure 3: Architecture of (a) a typical three-layer multi-layer perceptron (MLP) neural network and (b) a typical a long-short time
830   **memory (LSTM) network. Ψ_i denotes the sigmoid transfer function, $W_{i,j}$ represent connection weights between the input layer and the hidden layer, $I_{j,k}$ represent connection weights between the hidden layer and the output layer. x_t, c_t, and h_t represent the standardized input variable, hidden gate and cell gate at the current time t.**
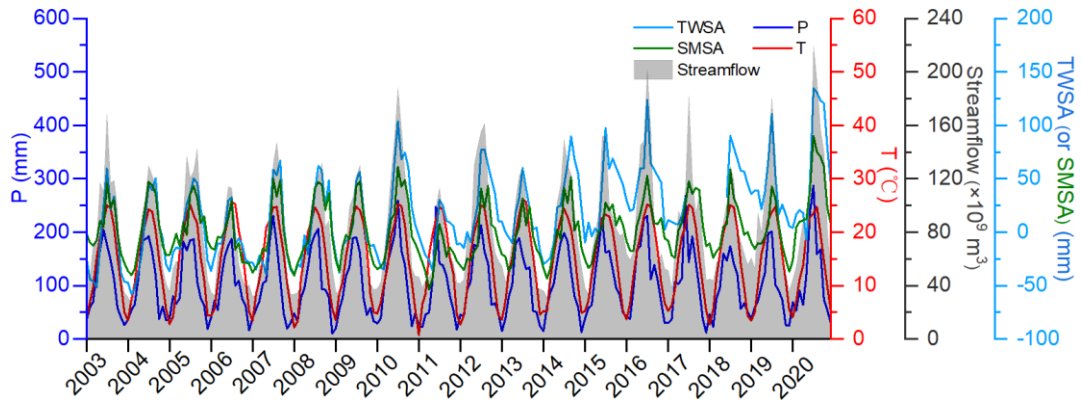
Figure 4: Monthly time series of precipitation (P, mm), temperature (T, °C), terrestrial water storage anomaly (TWSA, mm), soil moisture storage anomaly (SMSA, mm) and streamflow (×10⁹ m³) across the YRB during 2003-2020. Streamflow data is obtained at the Datong hydrological station (shown in Figure 1). YRB = Yangtze River Basin.

835
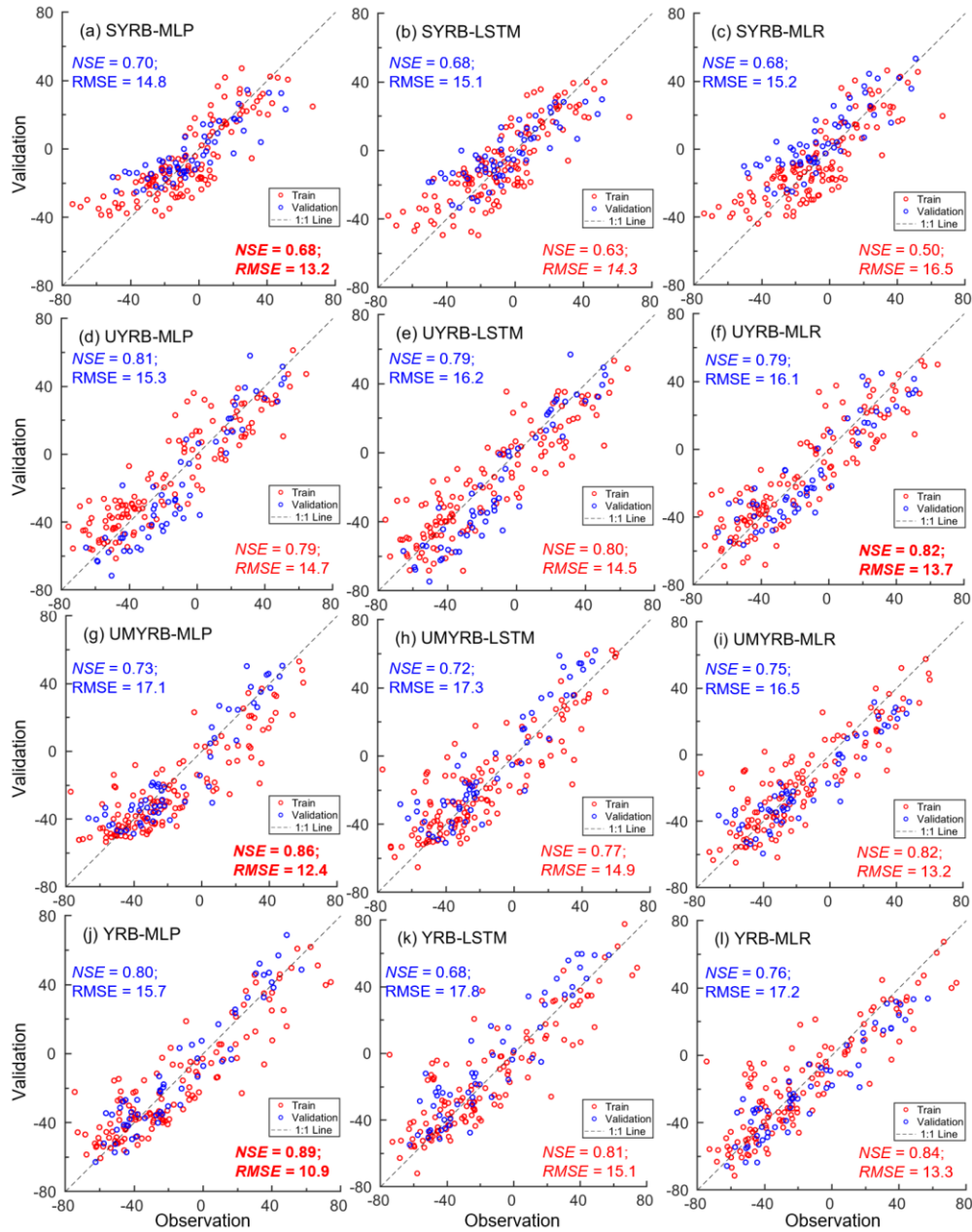
Figure 5: Comparison between monthly TWSA derived from GRCACE/GRACE-FO satellite data (observation) and that simulated by different models (validation) for (a-c) the SYRB, (d-f) the UYRB, (g-i) the UMYRB and (j-l) the YRB respectively during 2003-2020 with showing statistics of the comparison including root mean square errors (RMSE) (mm/month) and Nash-Sutcliffe efficiency (NSE). Note that TWSA shown in this figure are detrended because hydro-climatic factors may not fully simulate all the long-term trends. The models showing the best performance in simulating TWSA during the validation periods have been bold for each region. SYRB = Source regions of Yangtze River Basin; UYRB = Upper regions of Yangtze River Basin; UMYRB = Upper and middle regions of Yangtze River Basin; YRB = Yangtze River Basin.
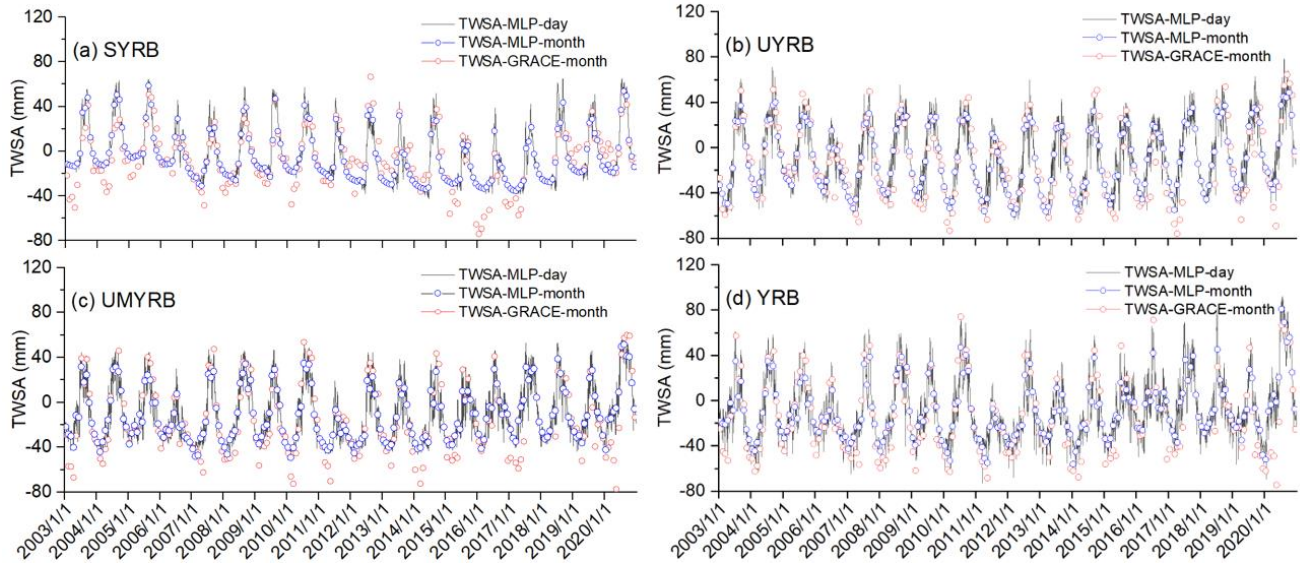
845

Figure 6: Daily (TWSA-MLP-day) and monthly (TWSA-MLP-month) time series of TWSA simulated by the MLP model for (a) the SYRB, (b) the UYRB, (c) the UMYRB and (d) the YRB respectively during 2003-2020. Note that monthly TWSA estimates derived from GRACE/GRACE-FO satellite data (TWSA-GRACE-month) shown in this figure are detrended because hydro-climatic factors may not fully simulate their long-term trends. TWSA = Terrestrial water storage anomaly; MLP = Multi-layer
850 **perceptron neural network; SYRB = Source regions of Yangtze River Basin; UYRB = Upper regions of Yangtze River Basin; UMYRB = Upper and middle regions of Yangtze River Basin; YRB = Yangtze River Basin.**
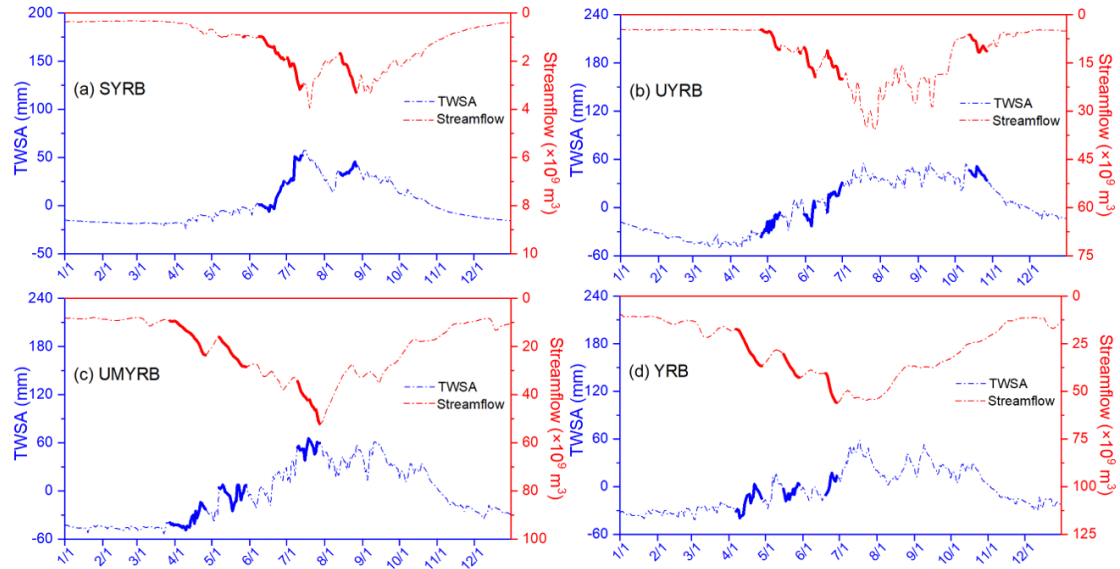
Figure 7: Daily TWSA temporally downscaled by the MLP model versus streamflow during flood events across (a) the SYRB, (b) the UYRB, (c) the UMYRB and (d) the YRB respectively in 2010. The bold blue dash lines and bold red dash lines represent daily TWSA and streamflow during the period between the beginning and end of each runoff event. TWSA = Terrestrial water storage anomaly; MLP = Multi-layer perceptron neural network; SYRB = Source regions of Yangtze River Basin; UYRB = Upper regions of Yangtze River Basin; UMYRB = Upper and middle regions of Yangtze River Basin; YRB = Yangtze River Basin.
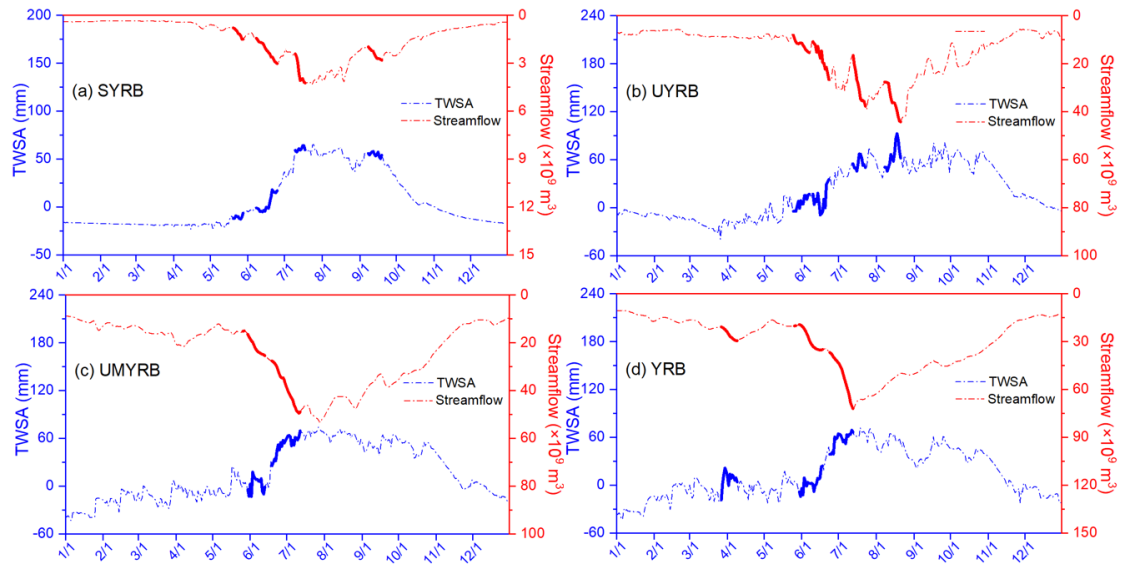
Figure 8: Same as Figure 7 but in 2020.
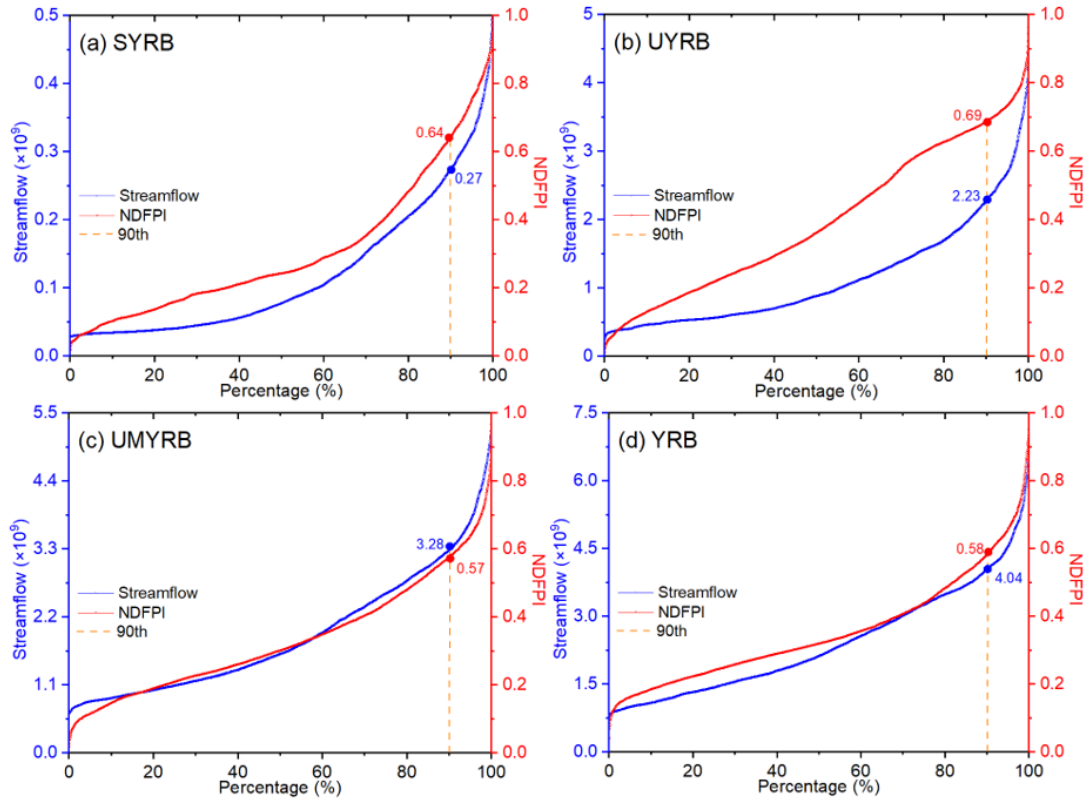
Figure 9: Percentile duration curves of daily streamflow observations and NDFPI for the 90th percentile floods across (a) the SYRB, (b) the UYRB, (c) the UMYRB and (d) the YRB respectively during 2003-2020. The red dots and blue dots represent threshold values of daily streamflow and NDFPI for the 90th percentile floods across different regions. SYRB = Source regions of Yangtze River Basin; UYRB = Upper regions of Yangtze River Basin; UMYRB = Upper and middle regions of Yangtze River Basin; YRB = Yangtze River Basin; NDFPI = Normalized daily flood potential index.
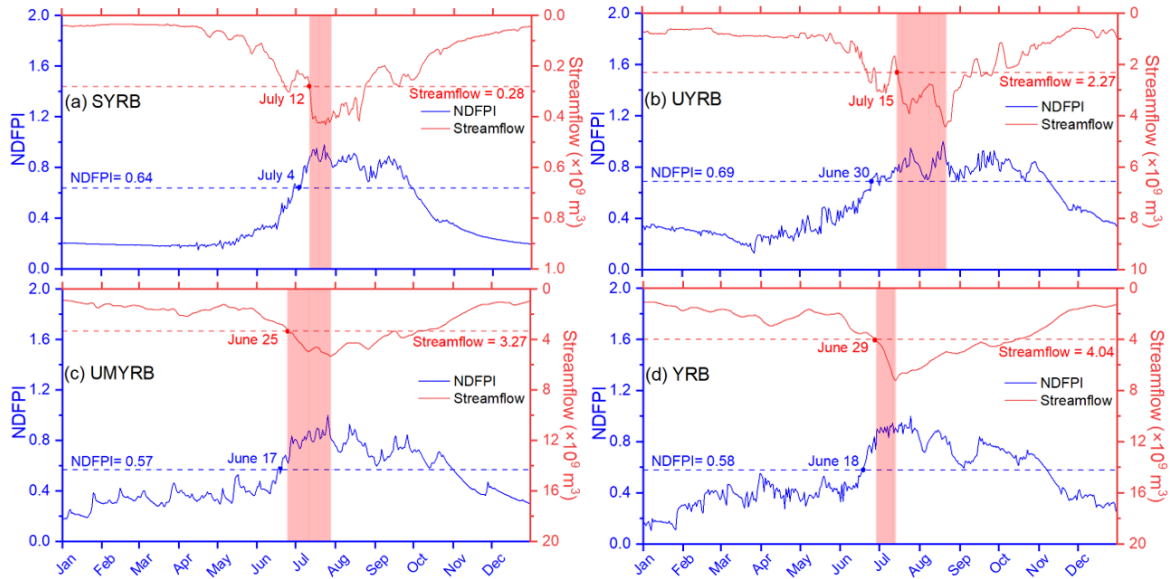
Figure 10: Comparison between basin averaged NDFPI and daily streamflow observations for the 90th percentile floods in 2020 across (a) the SYRM (observed at Shigu station), (b) the UYRB (observed at Yichang station), (c) the UMYRB (observed at Hankou station) and (d) the YRB (observed at Datong station). Pink rectangles denote the duration period between the thresholds of daily streamflow for the 90th percentile floods and peak streamflow observed at the controlling hydrological stations over different regions. The thresholds of daily streamflow and NDFPI for the 90th percentile floods are represented by the red dash lines and blue dash lines respectively. Note that the scales of streamflow shown in each figure are not always same. SYRB = Source regions of Yangtze River Basin; UYRB = Upper regions of Yangtze River Basin; UMYRB = Upper and middle regions of Yangtze River Basin; YRB = Yangtze River Basin; NDFPI = Normalized daily flood potential index.

870